Mathematical–Physical Framework for Retrieval of Rain DSD Properties from Dual-Frequency Ku–Ka-Band Satellite Radar

KWO-SEN KUO

Caelum Research Corporation, and NASA Goddard Space Flight Center, Greenbelt, Maryland

ERIC A. SMITH

NASA Goddard Space Flight Center, Greenbelt, Maryland

ZIAD HADDAD AND EASTWOOD IM

Radar S&E, NASA Jet Propulsion Laboratory, California Institute of Technology, Pasadena, California

TOSHIO IGUCHI

Global Environment Division, Communications Research Laboratory, Tokyo, Japan

ALBERTO MUGNAI

Institute of Atmospheric Science and Climate, National Research Council, Rome, Italy

(Manuscript received 27 August 2002, in final form 13 April 2004)

ABSTRACT

In developing the upcoming Global Precipitation Measurement (GPM) mission, a dual-frequency Ku–Ka-band radar system will be used to measure rainfall in such a fashion that the reflectivity ratio intrinsic to the measurement will be sensitive to underlying variations in the drop size distribution (DSD) of rain. This will enable improved techniques for retrieving rain rates, which are dependent upon several key properties of the DSD. This study examines this problem by considering a three-parameter set defined by liquid water content (W), DSD effective radius (r_e), and DSD effective variance (v_e). Using radiative transfer simulations, this parameter set is shown to be related to a radar reflectivity factor and specific attenuation in such a fashion that details of the DSDs are immaterial under constant W, and thus effectively represent important variations in DSD that affect rain rate but with a minimal number of parameters. The analysis also examines the effectiveness of including some measure of mean Doppler fall velocity of raindrops ($\overline{v}$), given that the fundamental properties of a given precipitation situation are uniquely defined by a combination of a drop mass spectrum and drop vertical velocity spectrum. The results of this study have bearing on how future dual-frequency precipitation retrieval algorithms could be formulated to optimize the sensitivity to underlying DSD variability, a problem that has greatly upheld past progress in radar rain retrieval.

1. Introduction

Toward the end of the twentieth century, in November 1997, earth science witnessed the first attempt to measure rainfall from space with a rain radar system. Notably, the attempt proved highly successful and has inspired a new remote sensing discipline accompanied by a new generation of science experts focused on new problems born from the technology [see Meneghini and Kozu (1990) and Okamoto et al. (2001) for background on spaceborne rain radar technology]. The first rain radar was launched on Thanksgiving Day on the Tropical Rainfall Measuring Mission (TRMM) observatory—aptly named the precipitation radar (PR). The PR was developed by the National Space Development Agency of Japan (NASDA) in collaboration with Japan's Communications Research Laboratory (CRL). The instrument is a Ku-band (13.8 GHz) noncoherent radar, using a 2 m $\times$ 2 m phased-array antenna configured with 128 slotted waveguides mounted within an aluminum frame and deployed as a cross-track electronic scanning system on the underside of the TRMM satellite bus in flight (see Okamoto et al. 1988; Nakamura et al. 1990; Kummerow et al. 1998; Meneghini et al. 2000; Kozu et al. 2001).

Corresponding author address: Kwo-Sen Kuo, NASA GSFC, GEST/Caelum, Mail Stop 912.1, Greenbelt, MD 20771.
E-mail: kskuo@radar.gsfc.nasa.gov

The foremost advantage of the PR measurements is their representation of the three-dimensional structures of precipitating storms, including tropical cyclones, baroclinic midlatitude cyclones, squall lines, supercells, warm rain mountain clouds, and various other types of convective, stratiform, and mixed-type precipitating cloud environments (e.g., see, Shin et al. 2000; Short and Nakamura 2000; Petersen and Rutledge 2001). The second advantage of PR measurements is that they provide a completely new methodology for estimating global rain rates from an unambiguous top-down radar view, beyond what has been possible from passive microwave radiometers dating back to the early 1970s (see Testud et al. 1992; Iguchi and Meneghini 1994; Haddad et al. 1997b; Iguchi et al. 2000).

Regardless of the significant scientific gains that have been made possible by PR measurements, there are still significant improvements that can be achieved with more advanced spaceborne radar systems. This study examines some of those possibilities, particularly those associated with the use of a dual-frequency radar system capable of generating good dynamic range for reflectivity ratio (see Meneghini et al. 2001) and those associated with the inclusion of a broadband Doppler capability (first two spectral moments) for estimation of raindrop fall velocities (e.g., Amayenc et al. 1993; Tanelli et al. 2002). Our analysis attempts to look ahead to the new generation of spaceborne radar technology as encompassed in the PR-2 aircraft radar program at the Jet Propulsion Laboratory (JPL), a dual-frequency Ku–Ka-band coherent polarimetric radar system (see Durden et al. 1994; Im et al. 2002), and the dual-frequency precipitation radar (DPR) satellite development program of NASDA and CRL (Japan's PR follow-up program), consisting of a dual-frequency Ku–Ka-band noncoherent single-pol radar system for use with the now evolving Global Precipitation Measurement (GPM) mission (see Smith et al. 2004). (The JPL PR-2 airborne instrument serves as the DPR prototype but carrying additional capabilities of Doppler agility and dual-polarization for enhanced multiparameter measurements.)

2. Brief review of dual-frequency methods

Since it was pointed out, as early as 1953, that a single radar measurement was inadequate for accurate rain-rate retrieval (Twomey 1953), researchers have been making use of multiparameter radar measurements for the retrieval of rainfall characteristics (e.g., Chandrasekar et al. 1993). Multiparameter techniques can be classified into those employing multiple polarizations, multiple frequencies, Doppler signals, or hybrids, which employ some combination of the aforementioned (see Nakamura and Inomata 1992). The multipolarization methods exploit the fact that raindrops are often spheroids rather than spheres and that their deviation from sphericity is size dependent. Thus, raindrops reflect more electromagnetic waves polarized along the major axes of their elliptical cross sections than those polarized along their minor axes. As the raindrop increases in size, the eccentricity of its elliptical cross section also increases. Therefore, disparity between polarizations becomes an indicator to the size of a raindrop.

Although multipolarization methods may provide capability for distinguishing hydrometeor phase, especially identification of large frozen aggregates undergoing initial melting, a raindrop's elliptical cross section is often near parallel to the local vertical axis along which spaceborne radars are most likely to observe. Therefore, nonsphericity of raindrops, and hence polarization, ceases to be a robust estimator of raindrop size. For this reason and in the context of GPM, in this paper we only address techniques involving multiple frequencies and Doppler signals.

The problem of radar rainfall retrieval from space can be described as follows. Suppose the range gates are numbered top-down from 1 to N, and at each range gate we have one reflectivity measurement (perhaps an average of a number of pulses) for each of M frequencies. We denote the reflectivity measurement at the ith frequency from the jth gate as Z_{ij}. The major factor determining the value of Z_{ij} is the hydrometeor mix within the range gate. Assuming that all hydrometeors are in liquid phase, the drop size distribution (DSD) of the water droplets, denoted $n_j(r)$, plays a crucial role in radar rainfall retrieval.

In the most general case, the measurement of DSD within any given range gate is assumed independent to that of any other range gate. Therefore, the number of measurements—that is, frequencies in the context of our discussion—needed per range gate is dictated by the number of parameters required to adequately describe the DSD. For example, if a two-parameter distribution such as the exponential distribution is assumed, we need at least two independent measurements per layer to be able to resolve the DSD, that is, $M \geq 2$.

In this sense, the oft-referenced dual-wavelength attenuation technique proposed by Eccles and Mueller (1971) is not truly a dual-measurement method, since only the attenuation in the 3-cm signal is used for rainfall estimates. Plagued by uncertainty in calibration, the reflectivity factor is discarded by this method. Therefore, the uncertainty in the power-law relationship between liquid water content and attenuation is still dominated in much the same manner as the single-frequency Z–R relationship by variations in the drop size spectra. On the other hand, the methods suggested by Atlas (1954) and investigated in more detail with different assumptions by Goldhirsh and Katz (1974) are actual two-measurement techniques, where two pieces of information derived from the measurements are used to determine two parameters of the rain DSD. However, unlike the method of Eccles and Mueller (1971), these methods are prone to error in calibration since the calibration uncertainty remains in the reflectivity factor, which is used to derive one of the DSD parameters. One

way to overcome uncertain calibration is to use path-integrated attenuation as a constraint, which may be derived in two ways. One uses an estimate of the surface echo (Meneghini et al. 1983, 1987, 2000; Kozu et al. 1991; Marzoug and Amayenc 1991, 1994; Li et al. 2002), while the other uses concurrent passive microwave measurements near or at the same frequency (Kozu and Nakamura 1991; Meneghini et al. 1997; Smith et al. 1997; Li et al. 2002).

The method developed by Fujita and colleagues (Fujita 1983; Fujita et al. 1985) typifies another class of dual-frequency algorithms. They relate both the equivalent reflectivity factor and the specific attenuation to rain rate in power laws. The rain rates are then retrieved in a least squares manner using the power laws in conjunction with the measured equivalent reflectivity factors. Other than the calibration uncertainty, this method is also prone to errors in the power laws that involve rain rate directly. This will be made clear in a later discussion.

In the authors' view, the crux of the rain-rate retrieval problem from space reduces to choosing a minimal set of characteristic DSD parameters that 1) uniquely determine the radar measurables—hence are retrievable with these measurements, and 2) are applicable to a wide range of DSDs, preferably universally (see Haddad et al. 1996, 1997a; Testud et al. 2001).

Atlas (1954) and Atlas and Chmela (1957) made a strong case for the use of medium-volume diameter, liquid water content, and a measure of the breadth of the DSD as the characteristic parameters (to be discussed). When Rayleigh scattering is valid, these parameters meet the two requirements. However, the balance between scientific requirements and practical considerations limits the frequencies usable by a spaceborne radar to approximately 10–95 GHz, for which the Rayleigh scattering approximation is invalid for most precipitating hydrometeors. Therefore, we are making the case for another set of characteristic parameters suitable for such frequencies. In addition, we explore the improvement that can be made to rain retrieval with the addition of a measurement of Doppler mean velocity.

Section 3 introduces necessary background for the analysis, while section 4 presents the results of radiative transfer simulations needed to demonstrate the validity of our ideas. Section 5 then discusses the implications related to these ideas, with final conclusions offered in section 6.

3. Background

a. Bimodal modified gamma DSD model

We first note that we use ''true'' or ''actual'' distribution to mean the measured DSD, a recording of the number of particles for each prescribed size bin. A DSD model, however, is a mathematical expression fitted to the actual size distribution in order to concisely describe the DSD using a small number of parameters. To ensure that the resultant characteristic DSD parameters are applicable to a wide range of DSD distributions, we need to start with a sufficiently general DSD model for our analysis. The DSD model used in this analysis is a ''bimodal modified gamma distribution,'' involving two modified gamma distributions with the same μ and κ constants (Deirmendjian 1969):

$$
\begin{aligned}
n(r) = {} & G\left(\frac{\mu + 1}{\kappa}, z_{1,\min}, z_{1,\max}\right)^{-1} \\
& \times \kappa\left(\frac{r}{r_{c,1}}\right)^{\mu} \exp\left[-\left(\frac{r}{r_{c,1}}\right)^{\kappa}\right]\left(\frac{fN_T}{r_{c,1}}\right) \\
& + G\left(\frac{\mu + 1}{\kappa}, z_{2,\min}, z_{2,\max}\right)^{-1} \\
& \times \kappa\left(\frac{r}{r_{c,2}}\right)^{\mu} \exp\left[-\left(\frac{r}{r_{c,2}}\right)^{\kappa}\right]\left[\frac{(1 - f)N_T}{r_{c,2}}\right], \quad (1)
\end{aligned}
$$

where N_T is the total number concentration, f is a fraction between 0 and 1, $r_{c,1}$ and $r_{c,2}$ are characteristic radii in the first and second modified gamma distributions in which $r_{c,1} < r_{c,2}$, and the function G is given by

$$
\begin{aligned}
G\left(\frac{\mu + 1}{\kappa}, z_{\min}, z_{\max}\right) = {} & \left[\gamma\left(\frac{\mu + 1}{\kappa}, z_{\max}\right)\right. \\
& \left. - \gamma\left(\frac{\mu + 1}{\kappa}, z_{\min}\right)\right], \quad (2)
\end{aligned}
$$

where γ is the incomplete gamma function. The reader is referred to appendix A for a detailed discussion of γ and for the definitions of its parameters and constants. The raindrops are assumed spherical in this analysis, which can be relaxed in future studies.

The most distinctive trait of this distribution model is its generality; in all, there are a total of eight adjustable parameters. By setting restrictions on these parameters, it may be reduced, in decreasing order of complexity, to the modified gamma, the gamma, and the exponential distributions. In essence, it explicitly encompasses all popular DSD models used in rainfall research except for the lognormal distribution. Most importantly, it is capable of simulating bimodal features often observed in DSD measurements (Czerwinski and Pfisterer 1972). We emphasize that it is not our intention to use this complex DSD model directly for retrieval purpose; on the contrary, it is used to demonstrate the superior applicability of only three characteristic DSD parameters (W, r_e, and v_e) defined later.

Since integration of the DSD multiplied by some power of the radius frequently appears in quantities related to radar retrieval, we note that

TABLE 1. Definitions of terms and units.

Symbol	Units	Definition	Description
σ_b	cm^2		Backscattering cross section
σ_e	cm^2		Extinction cross section
ρ_w	g cm^{-3}		Density of water
λ	cm		Wavelength
m		$m = m_R - im_I$	Complex index of refraction
K		$K = \dfrac{m^2 - 1}{m^2 + 2}$	Dielectric factor
r	cm		Raindrop radius
$n(r)$	m^{-3} cm^{-1}		Drop size distribution (DSD)
$v(r)$	m s^{-1}		Velocity distribution
Z_e	mm^6 m^{-3}	$Z_e = \dfrac{10^6\lambda^4}{\pi^5\lvert K_w\rvert^2}\displaystyle\int_{r_{\min}}^{r_{\max}} \sigma_b(r)n(r)\,dr$	Equivalent radar reflectivity factor
Z	mm^6 m^{-3}	$Z = 64 \times 10^6 \displaystyle\int_{r_{\min}}^{r_{\max}} r^6 n(r)\,dr$	Radar reflectivity factor (Rayleigh approximation)
k	dB km^{-1}	$k = 0.434 \displaystyle\int_{r_{\min}}^{r_{\max}} \sigma_e(r)n(r)\,dr$	Specific attenuation

$$\int_{r_{\min}}^{r_{\max}} r^p n(r)\,dr = H(p)N_T r_{c,1}^p, \tag{3}$$

where

$$H(p) \equiv H\left(p, f, \mu, \kappa, r_{c,1}, \frac{r_{c,2}}{r_{c,1}}, r_{\min}, r_{\max}\right) = f\frac{G\left(\dfrac{\mu + p + 1}{\kappa}, z_{1,\min}, z_{1,\max}\right)}{G\left(\dfrac{\mu + 1}{\kappa}, z_{1,\min}, z_{1,\max}\right)} + (1 - f)\frac{G\left(\dfrac{\mu + p + 1}{\kappa}, z_{2,\min}, z_{2,\max}\right)}{G\left(\dfrac{\mu + 1}{\kappa}, z_{2,\min}, z_{2,\max}\right)}\left(\frac{r_{c,2}}{r_{c,1}}\right)^p. \tag{4}$$

Appendix A provides details of this derivation.

b. Integral quantities involving DSD

Using Eqs. (3) and (4), W is determined by

$$W = \frac{4}{3}\pi\rho_w \int_{r_{\min}}^{r_{\max}} r^3 n(r)\,dr = \frac{4}{3}\pi\rho_w H(3)N_T r_{c,1}^3, \tag{5}$$

where ρ_w is the density of water. Therefore, once the characteristic radius $r_{c,1}$ is determined, various Ws can be obtained by adjusting the total number concentration N_T, provided that the H function remains unchanged.

The rain rate R which is the quantity of utmost concern in this study, is also an integral involving the size distribution:

$$R \equiv 4.8\pi \int_{r_{\min}}^{r_{\max}} v(r)r^3 n(r)\,dr, \tag{6}$$

where $v(r)$ is the terminal or fall velocity of a raindrop of radius r, also defined as the "velocity distribution" of raindrops. The dependence of $v(r)$ on r, needed for the integration, is subject to the influence of its environment and, therefore, is not unique. In most simulations (e.g., Atlas and Ulbrich 1977; Ulbrich 1986, 1992; Meneghini and Kozu 1990; Meneghini et al. 1992; Haddad et al. 1996), $v(r)$ is assumed to be the same as the terminal velocity of water droplets in stagnant air, denoted by $v_0(r)$, for example, as measured by Gunn and Kinzer (1949) in the laboratory.

Several velocity distribution models have been developed from the latter study to express the dependence of $v_0(r)$ on r (e.g., Spilhaus 1948; Atlas and Ulbrich 1977; Lhermitte 1988; Gossard et al. 1992). Here, we make use of the formulation given by Atlas and Ulbrich (1977) for its mathematical simplicity and relatively good performance (see Meneghini and Kozu 1990):

$$v_0(r) \approx 28.11r^{0.67}, \tag{7}$$

where r is in centimeters, and $v_0(r)$ has units of meters per second.

Two radar measurements investigated in this study are the reflectivity factor Z_e and the specific attenuation k whose mathematical definitions are

TABLE 2. Distribution parameters for the five categories of DSDs.

Category	Type	f	$r_{c,2}/r_{c,1}$	$r_{\max}$ (mm)
1	Monomodal	1	1	20
2	Monomodal	1	1	15
3	Bimodal	0.5	5	15
4	Bimodal	0.3	5	15
5	Bimodal	0.3	10	15

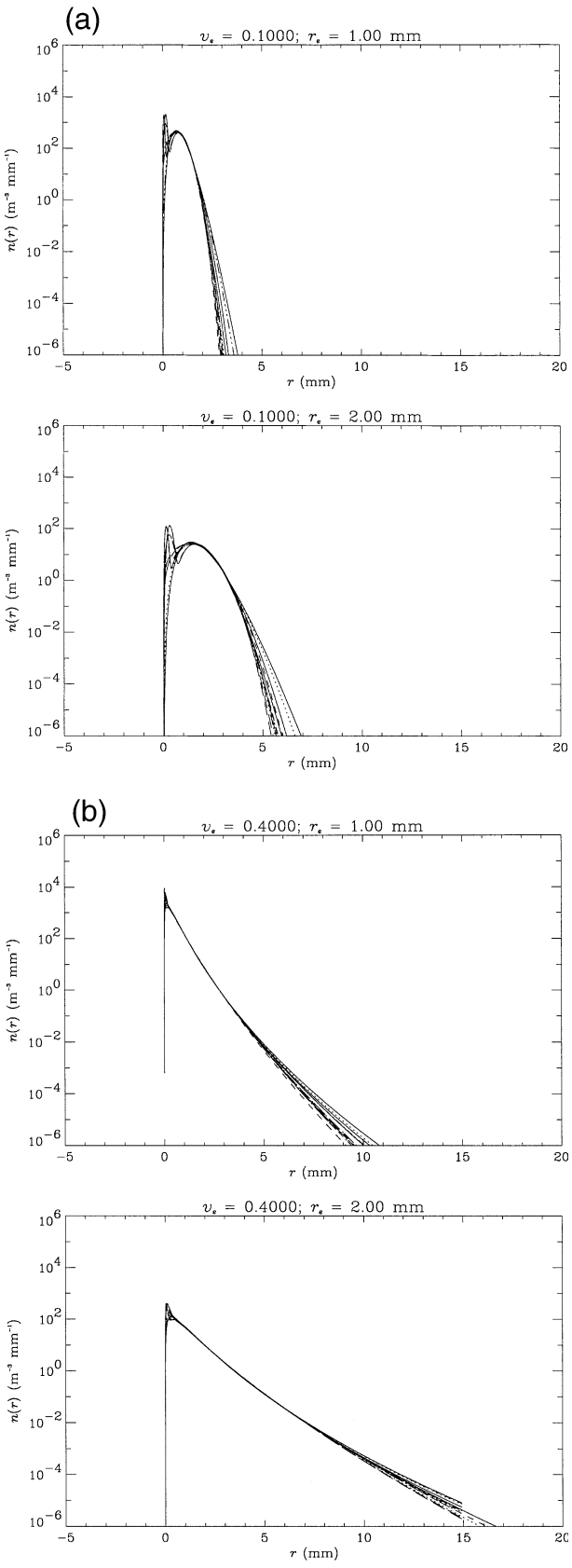

FIG. 1. (a) Fifteen drop size distributions, generated using Eq. (1), with the same effective radii of (top) 1 and (bottom) 2 mm and the same effective variance of 0.1. (b) Same as (a), except for effective variance of 0.4.

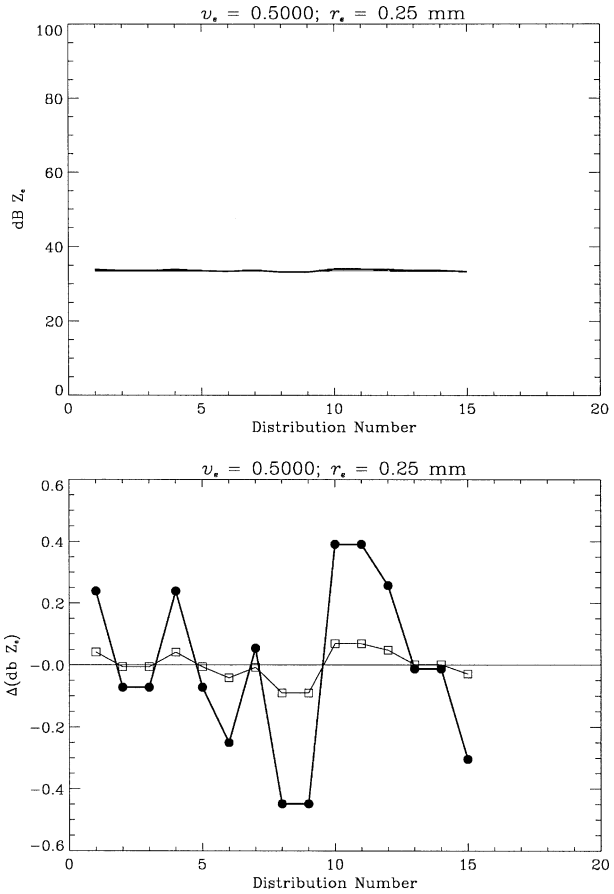

FIG. 2. Variations of equivalent radar reflectivity factor, Z_e, among 15 distributions with (top) the same effective radius of 0.25 mm and effective variance of 0.5 and (bottom) deviations from mean.

$$Z_e = \frac{10^6 \lambda^4}{\pi^5 |K_w|^2} \int_{r_{\min}}^{r_{\max}} \sigma_b(r) n(r)\, dr \qquad \text{and} \qquad (8a)$$

$$k = 0.434 \int_{r_{\min}}^{r_{\max}} \sigma_e(r) n(r)\, dr. \qquad (8b)$$

Table 1 provides definitions of terms and units. Similar to rain rate, both Z_e and k are integrals involving the product of the DSD and some function of the radius. Therefore, it is natural and logical to relate these quantities. In fact, this attempt has met with some limited success, usually in the form of power laws such as $R = aZ_e^b$ or $Z = \alpha k^\beta$, where a, b, α, and β are often determined empirically (e.g., Eccles 1979 and Battan 1973 and references therein).

As noted by Haddad et al. (1995), the usefulness of

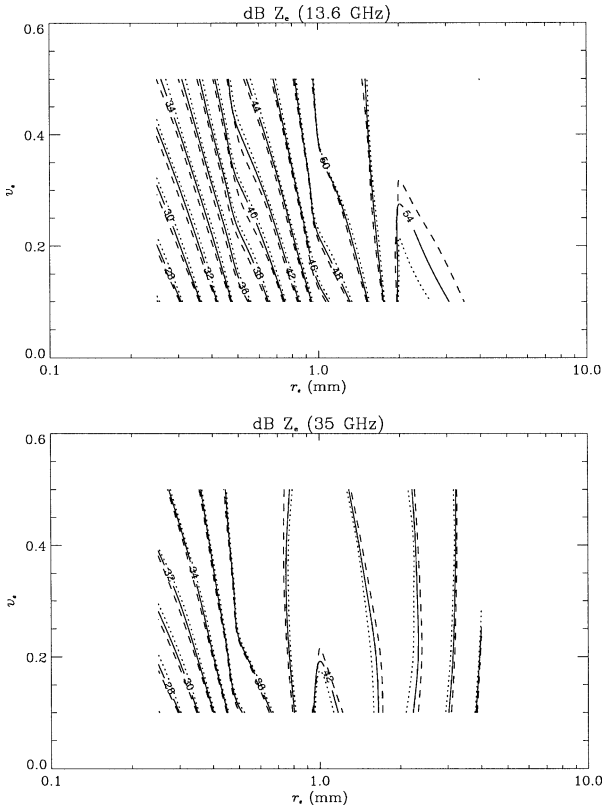

FIG. 3. Contours of equivalent radar reflectivity factor at (top) 13.6 and (bottom) 35 GHz as a function of effective radius and effective variance when holding liquid water content constant at 1 g m^{-3}. Solid contours are the mean of 15 distributions, while dotted and dashed contours denote minimum and maximum, respectively.

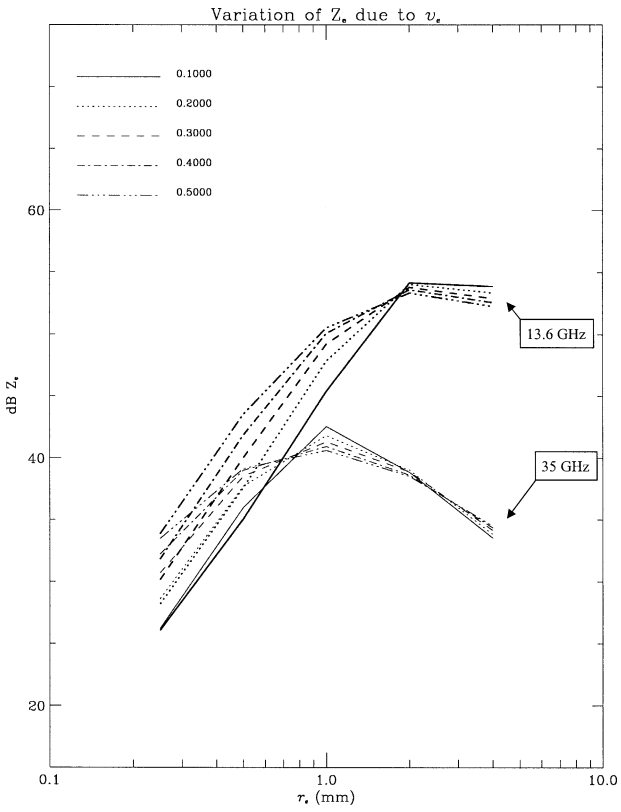

FIG. 4. Effect of effective variance on equivalent radar reflectivity. Thick lines are for 13.6 GHz, while thin ones are for 35 GHz.

power laws is impaired by the nonunique nature of the problem. Examining Eqs. (8a) and (8b), we recognize that Z_e and k are proportional to the total backscattering and extinction cross sections, respectively. Thus, different DSDs may produce the same total backscattering or extinction cross section, hence the same Z_e or k. As a matter of fact, given a Z_e or k, there is an infinite number of DSDs that satisfy the underlying relationships. Since, in general, the quantity $v(r)r^3$ in the integrand of the definition for R has a different dependence on r from σ_b or σ_e, these DSDs may lead to different rain rates while producing the same Z_e or k. Therefore, within a mathematical framework, a single radar measurement cannot produce a completely accurate rain-rate estimate.

Twomey (1953) investigated the error in Z–R relationships caused by variations in the shape of the DSD, concluding ''radar methods can give only an approximate measure of precipitation rate; the value deduced from the radar echo may be in error by a factor of 2:1 either way.'' Atlas et al. (1984) also noted, ''In spite of the persuasive evidence . . . that one could not hope to determine R from a measurement of Z alone and a simple Z–R relationship, much of the community has persisted in this vain hope.'' Notably, many have sought appropriate Z–R relationships according to regional climatic or meteorological factors. This resulted in the 69 Z–R relationships reported in Battan (1973), confusing the issue when routine rain retrieval is being considered. For this reason, some have turned to multiparameter retrieval.

c. Estimated average Doppler velocity in stagnant air

Reexamining Eqs. (6), (8a), and (8b), one discovers that Z_e and k do not contain any information about $v(r)$, on which the estimate of rain rate depends. Earlier algorithms used the terminal velocity of raindrops in stagnant air, $v_0(r)$, in place of $v(r)$, for lack of an exact expression within a dynamically moving cloud environment. In reality, the dependence of terminal velocity on radius is complicated by in-cloud air motions. This is one of the reasons that dual-frequency methods, without incorporating terminal velocity information, have also achieved only limited success in estimating rain rates (see Walker et al. 1964).

The next simplest assumption to that of stagnant air is the influence of a homogeneous cloud updraft w such that

$$v(r) = v_0(r) - w. \tag{9}$$

Thus given an estimate of the mean Doppler velocity, $\overline{v}$, the cloud updraft is estimated by

$$w = \overline{v}_0 + \overline{v}, \tag{10}$$

where $\overline{v}_0$ is the mean Doppler velocity (terminal) that would be measured in absence of an updraft (Meneghini and Kozu 1990; Rogers 1984). Appendix B outlines how $\overline{v}_0$ is calculated.

d. Characteristic quantities of DSD

Even with full Doppler capability, it is uncertain whether it is possible to determine the DSD remotely (Rogers 1984). Moreover, full Doppler capability (i.e., Doppler spectra) does not appear practical for spaceborne radars in the near future. Fortunately, as previous investigations have shown, there is no need to know the size-bin-to-size-bin specifics of the rain DSD if it can be described by a known analytical distribution, such as exponential or gamma distributions.

Marshall and Palmer (1948) proposed the exponential raindrop size distribution

$$N(D) = N_0 \exp(-\Lambda D), \tag{11}$$

where D is the raindrop diameter. This is a two-parameter distribution in N_0 and Λ. In their expression, N_0 is assumed to be a constant independent of rain rate while Λ is parameterized according to $\Lambda = 41(R^{-0.21})$. This permits the retrieval of rain rate using a single reflectivity factor measurement.

Distribution models involving more parameters can be used when there are more than one simultaneous radar measurements. Ulbrich (1983) introduced a more generalized three-parameter gamma distribution,

$$N(D) = N_0 D^{\mu} \exp(-\Lambda D), \tag{12}$$

in which there is an algebraic relationship between μ and Λ, namely,

$$\Lambda D_0 \approx 3.67 + \mu, \tag{13}$$

where D_0 is the median volume diameter that satisfies

$$2\int_0^{D_0} D^3 N(D)\, dD = \int_0^{D_{\max}} D^3 N(D)\, dD, \tag{14}$$

and N_0 and μ are related as follows:

$$N_0 = C_N \exp(3.2\mu). \tag{15}$$

However, C_N assumes different values depending on whether Z–R relationships from Battan (1973) are used ($C_N = 6 \times 10^4$ m^{-3}) or the DSDs reported in Ulbrich and Atlas (1977) are used ($C_N = 1.5 \times 10^4$ m^{-3}).

If a third simultaneous remote measurable is available and the three-parameter gamma distribution is assumed, it is possible to achieve greater retrieval accuracy (see Atlas et al. 1984). But, what if the DSD is more complicated than can be captured by a gamma distribution? For example, a bimodal distribution is more representative as precipitating clouds transition from cumulus to cumulus congestus stages governed by stochastic coalescence.

A bimodal distribution such as the one suggested in Eq. (1) has no fewer than eight adjustable parameters. For retrieval purposes, determining all eight parameters requires at least eight simultaneous and independent measurements, which is generally impractical. However, we shall show that, in addition to W, only two characteristic quantities of the DSD are necessary to achieve accurate representation, regardless of the underlying theoretical distribution assumed. These are effective radius and effective variance as originally given by Hansen and Travis (1974):

$$r_e = \frac{\int_{r_{\min}}^{r_{\max}} r^3 n(r)\, dr}{\int_{r_{\min}}^{r_{\max}} r^2 n(r)\, dr} \quad \text{and} \tag{16a}$$

$$v_e = \frac{\int_{r_{\min}}^{r_{\max}} r^4 n(r)\, dr}{r_e^2 \int_{r_{\min}}^{r_{\max}} r^2 n(r)\, dr} - 1. \tag{16b}$$

Their numerical values for the bimodal modified gamma distribution, specified by Eq. (1), can be evaluated using

$$r_e = \frac{H(3)}{H(2)} r_{c,1} \quad \text{and} \tag{17a}$$

$$v_e = \frac{H(2)H(4)}{[H(3)]^2} - 1, \tag{17b}$$

in which details on these expressions are found in appendix A. Note that, in this paper, ''effective radius'' always means the effective radius of a DSD as defined by (16a) and should not be confused with the effective radius of a nonspherical drop since we assume spherical drops.

This concept of using quantities like r_e and v_e to characterize DSDs is not entirely new. As mentioned earlier, at wavelengths where the Rayleigh scattering approximation is valid, Atlas (1954) and Atlas and Chmela (1957), and references therein, found that the radar reflectivity factor Z (mm^6 m^{-3}) can be expressed using W (g cm^{-3}), D_0 (cm), and G as follows:

$$Z = \frac{6 \times 10^6}{\pi \rho_w} D_0^3 WG. \tag{18}$$

In this expression

$$G = \frac{\int_0^{D_{\max}} D^6 N(D)\, dD}{D_0^3 \int_0^{D_{\max}} D^3 N(D)\, dD}, \tag{19}$$

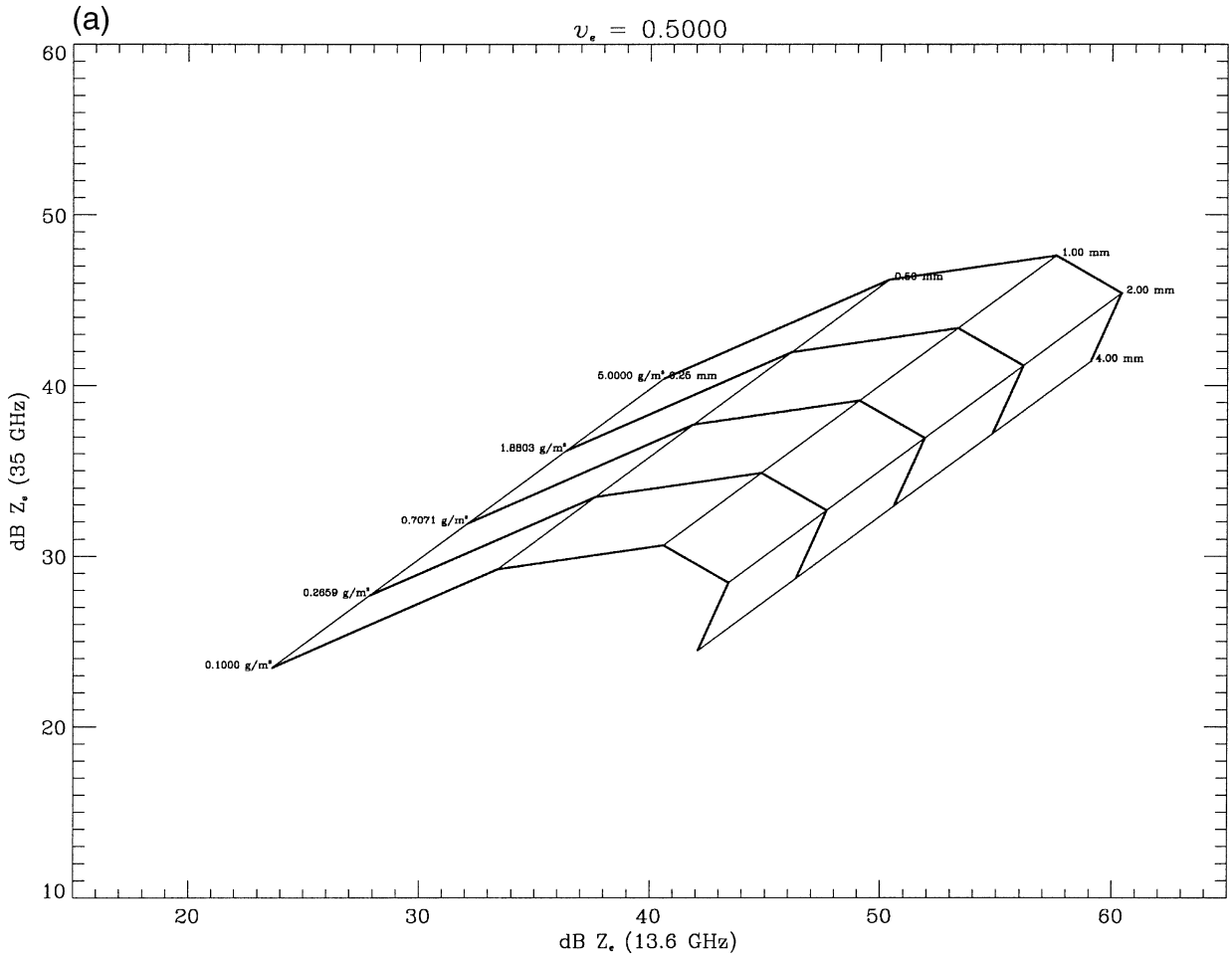

FIG. 5. Combined effects of liquid water content and effective radius on radar reflectivity factors at both 13.6 (abscissa) and 35 GHz (ordinate) for effective variance of (a) 0.5, (b) 0.3, and (c) 0.1.

which is a dimensionless quantity related to the breadth of the DSD.

One can easily verify that the above relationship—that is Eq. (18)—holds true for any size distribution without requiring approximations. That is, there is no need to cast the actual distribution into a model distribution such as exponential, lognormal, or otherwise, for the above relations to be valid. However, this is true only when the Rayleigh approximation is appropriate. For the 13.6- and 35-GHz frequencies under investigation (Ku–Ka band), Rayleigh scattering is not a valid assumption. Furthermore, it is difficult to express D_0 analytically when a more general distribution model such as the one given in Eq. (1) is used. Therefore, instead of D_0 and G, we choose for the purpose of this analysis to use r_e and υ_e as the characterizing quantities of the distributions.

Assuming a dual-frequency spaceborne radar with at least the Doppler capability to estimate $\overline{v}$, the first moment of the Doppler spectrum, a potential retrieval strategy may be as follows. First, W, r_e, and υ_e are retrieved from the dual-frequency equivalent reflectivity factors and specific attenuations using, say, a technique to minimize the differences between simulated and measured quantities. Then, $\overline{v}_0$ is estimated using the retrieved r_e and υ_e. In turn, Eqs. (9) and (10) are used to estimate the true fall speeds of raindrops, which are substituted in Eq. (6) for estimates of rain rate. For such a strategy to succeed, the essential requirements are 1) r_e and υ_e effectively represent an underlying DSD; 2) W, r_e, and υ_e are actually retrievable using available radar measurements; and 3) $\overline{v}_0$ can be determined uniquely by r_e and υ_e.

In the following subsections, we demonstrate the feasibility of this strategy using radiative transfer simulations. In section 4a, we first examine a wide variety of rain DSDs. In sections 4b and 4c, we demonstrate that both equivalent reflectivity factor and specific attenuation vary insignificantly once W, r_e, and υ_e are given, regardless of the specific distribution used. In section 4d, we show that given r_e and υ_e, $\overline{v}_0$ can be determined.

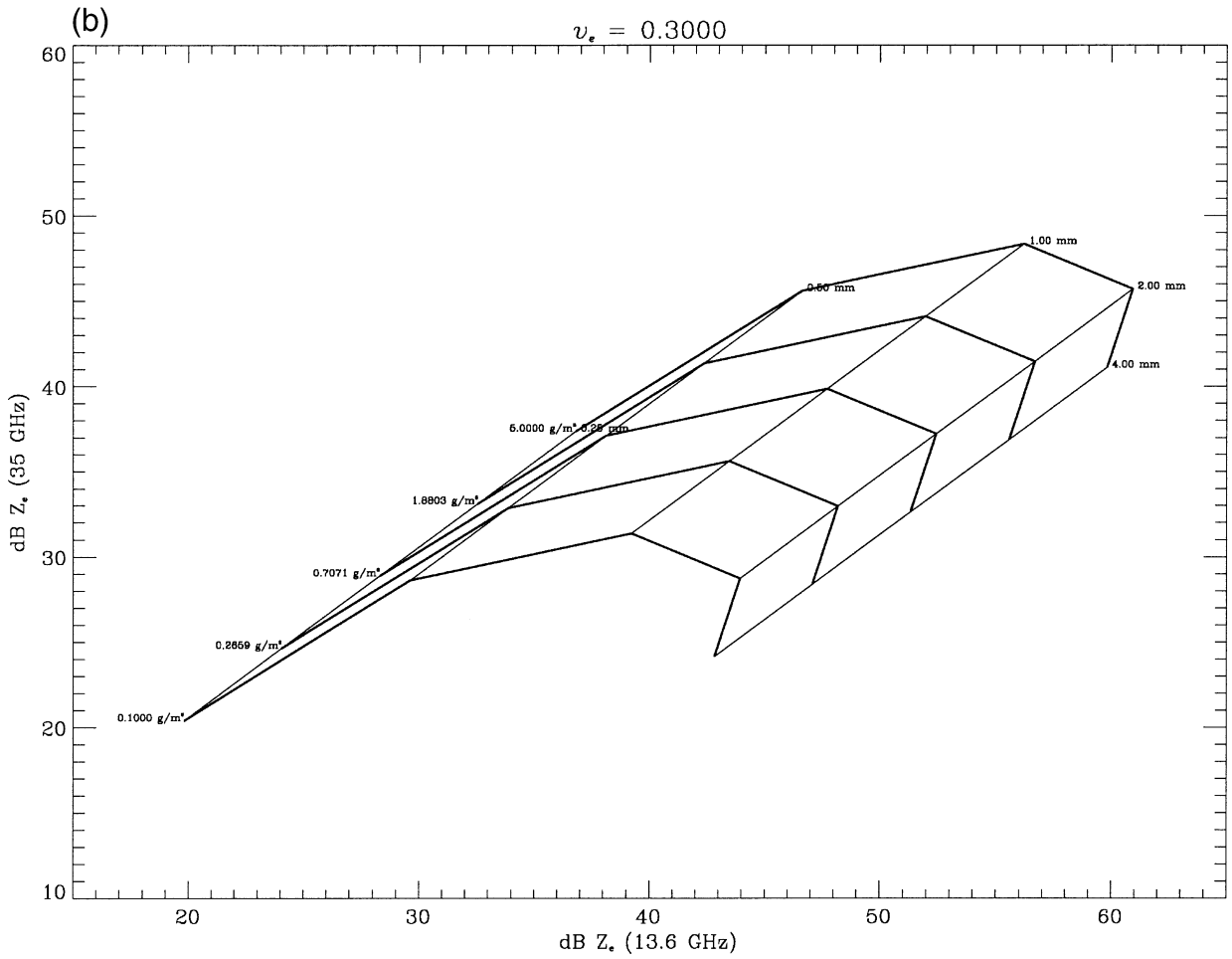

FIG. 5. (*Continued*)

4. Results

a. Drop size distribution

Our analysis is based on the bimodal modified gamma distribution, as defined in Eq. (1) above. (Appendix A provides additional details encompassing a variety of distributions in common use, i.e., the exponential distribution, the gamma distribution, and the modified gamma distribution.) We systematically vary the effective variance from 0.1 to 0.5 with an increment of 0.1, noting this quantity is dimensionless; for each effective variance we vary the effective radius among values of 0.25, 0.5, 1, 2, and 4 mm. For each value pair of effective variance and radius, a parameter-finding procedure determines μ, κ, $r_{c,1}$, and $r_{c,2}$ for a number of distributions yielding the desired effective variance and radius. This is carried out for each of the five distribution categories given in Table 2. The minimum radius for all distributions is $r_{\min} = 0$ mm. For each distribution category, three distributions are randomly selected from the distributions found by the parameter finder. Therefore, we examine a total of 15 different distributions for each effective variance and radius combination, three from each of the five categories. Since there are 25 (5×5) value pairs of effective variance and radius, this totals to 375 DSDs. In our later discussion, W for the distributions is held constant at 1 g m^{-3}, unless stated otherwise.

Figure 1a illustrates the 15 DSDs on a logarithmic scale for an effective variance of 0.1 and effective radii of 1 (upper panel) and 2 mm (lower panel). The distributions exhibit significant differences. Most of the variation in $n(r)$ lies at the smaller and larger radii. There is a stable middle section where the number concentrations of the various distributions are roughly the same. Since W is held constant at 1 g m^{-3}, the large differences in the number densities of smaller drops are offset by the small differences in the number densities of larger drops.

As the effective radius increases the distribution widens. Numerous smaller drops are replaced with fewer but larger drops. To maintain a constant W, the total number concentration, N_T, has to decrease as the effective radius increases as demanded by Eqs. (5) and (16a).

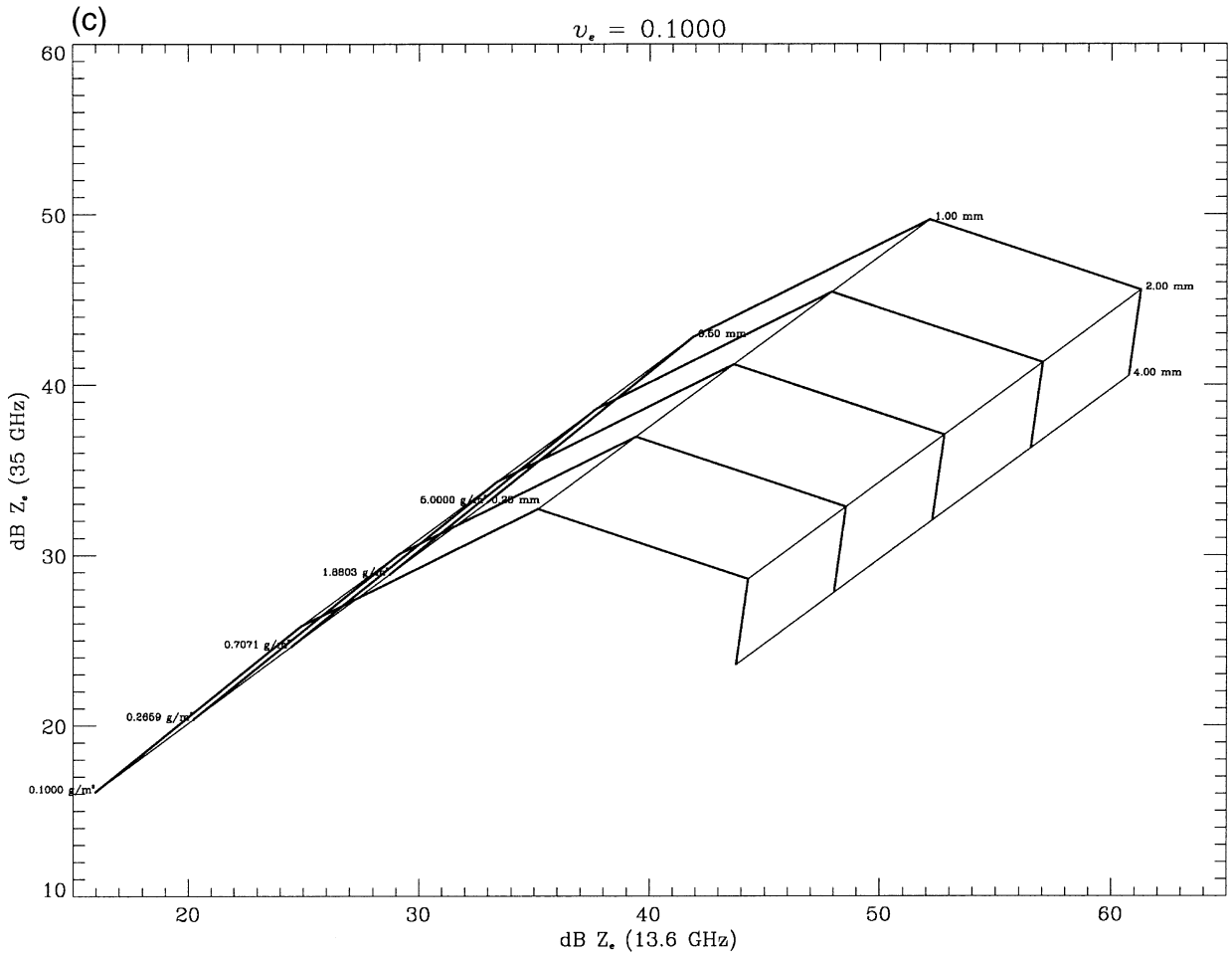

FIG. 5. (*Continued*)

For the same effective radius, the increase in effective variance appears to raise the tails of $n(r)$. For $r > r_m$, where r_m is the radius where the last maximum of $n(r)$ occurs—that is, $n(r) < n(r_m)$ for $r > r_m$—the shape of the $n(r)$ curve is convex when $\upsilon_e \leq 0.3$ and concave when $\upsilon_e \geq 0.3$. This can be seen by comparing Fig. 1a with Fig. 1b, which illustrates the distributions for the same effective radii but for an effective variance of 0.4.

b. Equivalent reflectivity factor

Although the distributions shown in Figs. 1a and 1b are quite different for the same effective variance and radius, the equivalent reflectivity factors for these distributions show little variation. The upper panel of Fig. 2 illustrates the reflectivity factors at 13.6 and 35 GHz for the 15 distributions with effective variance of 0.5 and effective radius of 0.25 mm. Since it is difficult to detect variations in the two plots, the deviations from their means are plotted in the lower panel. The deviations at 13.6 GHz are denoted by solid circles and connected with thick lines, while the open squares delineate deviations at 35 GHz connected by thin lines. Note the former exhibits a wider range of variation than the latter. The entire range is less than 1 dB, which is roughly the maximum variation that is observed in simulated data. In most cases, the range of variation is approximately 0.5 dB or less.

The variation of Z_e among distributions is depicted in a more comprehensive manner in the contour diagrams of Fig. 3. The solid lines contour the average equivalent reflectivity factors of the 15 distributions as a function of effective variance and radius, while the dotted lines contour the minimum of the distributions, and dashed lines contour the maximum. The proximity of the dotted and dashed lines with respect to their corresponding solid lines shows that, when W is constant, effective variance and radius are effective predictors of the equivalent reflectivity factors.

Moreover, one may estimate from these diagrams the variations due to the difference in effective variance. Holding effective radius constant, one finds that the increase in effective variance from 0.1 to 0.5 leads to an increase of as much as 6 to 8 dB in Z_e for both fre-

quencies. In general, the variation of Z_e caused by effective variance is larger for the smaller effective radii and for the lower frequency of 13.6 GHz.

Figure 4 demonstrates the effect of effective variance on the reflectivity factors from another perspective. The curves in this diagram plot the average reflectivity factor of the distributions as a function of effective radius for different effective variances that are represented using different line styles. The thinner lines are for the higher frequency while the thicker lines are for the lower frequency. We note that the effect of increasing effective variance is to reduce the extremes of the equivalent reflectivity factors; that is, the Z_e curve flattens out as effective variance increases. We also note that the equivalent reflectivity factors at both frequencies are roughly equal for effective radii smaller than 0.6 mm—when effective variance is 0.1. This region of overlap diminishes as the effective variance increases.

Another salient feature is that different effective radii may yield the same reflectivity factor, especially for the higher frequency. An effective radius smaller than ~1 mm may yield the same reflectivity factor as an effective radius greater than 1 mm; that is, there are multiple solutions to effective radius for the same equivalent reflectivity factor at 35 GHz. At 13.6 GHz, multiple solutions do not occur until the effective radius is larger than ~2 mm, near the upper bound of the analysis. This provides the rationale for using dual-frequency reflectivity factors for the retrieval of effective radius and W simultaneously, since the regions of multiple solutions occur at different effective radii for the two frequencies. When both frequencies are used together, the chance of encountering multiple solutions is minimized.

Figures 5a–c explore the feasibility and limitation of dual-frequency retrieval using equivalent reflectivity factors. The abscissas and ordinates are equivalent reflectivity factors at 13.6 and 35 GHz, respectively. The diagonal lines are isopleths of effective radii, with their values labeled at the top of the lines where they intersect the isopleth of W at 5 g m^{-3}. The isopleths of effective radii are traversed by isopleths of W whose values are labeled in the left-hand side of the plot along the isopleth of effective radius of 0.25 mm. The effective variances are 0.5, 0.3, and 0.1 for Figs. 5a, 5b , and 5c, respectively. The average of 15 distributions in each effective variance/radius category is used to plot the lines.

When effective variance equals 0.5 (Fig. 5a) there exists no region of multiple solutions. In other words, if a distribution has an effective variance of 0.5, its effective radius and W can be uniquely estimated using reflectivity factors at 13.6 and 35 GHz. However, when the effective variance is reduced to 0.3 (Fig. 5b), the area delimited by effective radii of 0.25 and 0.5 mm diminishes, hence reducing the resolvability for effective radii between them. At an effective variance of 0.2 (not shown) the two isopleths overlap. At this point, a distribution with an effective radius of 0.25 mm may be interpreted as a distribution with effective radius of 0.5 mm with lower W, and vice versa. This trend continues for an effective variance of 0.1 (Fig. 5c), where the 0.25-mm line encroaches into the area delimited by 0.5 and 1 mm. This is consistent with the results given in Fig. 4.

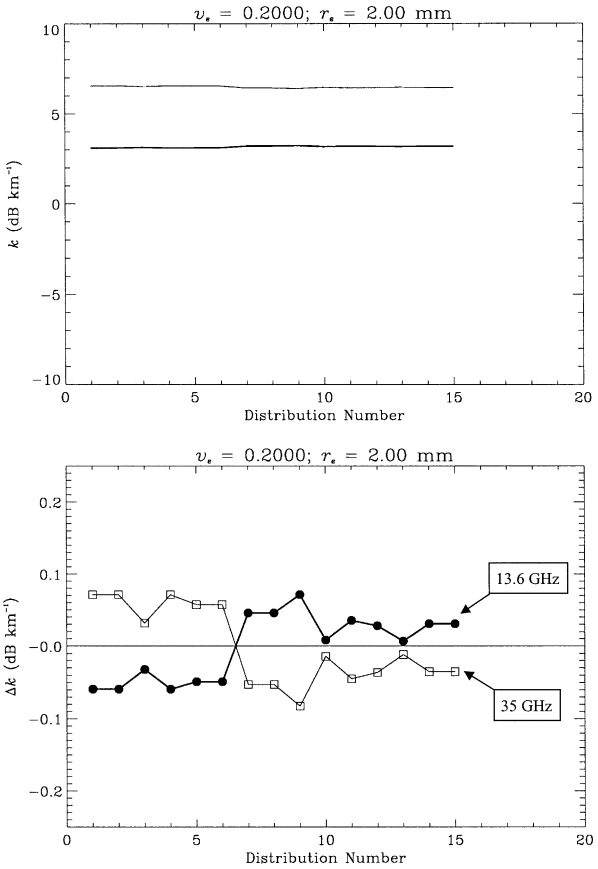

FIG. 6. Variations of specific attenuation k among 15 distributions with (top) the same effective radius of 2 mm and effective variance of 0.2 and (bottom) deviations from mean.

c. *Specific attenuation*

To avoid the uncertainty caused by the absolute calibration of the radar, specific attenuation is often preferable in the radar rain retrieval (Eccles 1979) since it does not depend on absolute radar calibration. This subsection examines the utility of specific attenuation, paralleling the analysis of equivalent reflectivity factors in the previous subsection. First, we investigate the variations of specific attenuation caused by varying DSDs. Similar to Fig. 2, Fig. 6 illustrates the specific attenuations at both frequencies for 15 distributions in five distribution categories (upper panel) and their deviations from their respective averages (lower panel) for effective variance of 0.2 and effective radius of 2 mm. The deviations are even less than those of reflectivity factors, with a total range of less than 0.2 dB km^{-1}.

Similar to Fig. 3, Fig. 7 illustrates the variations

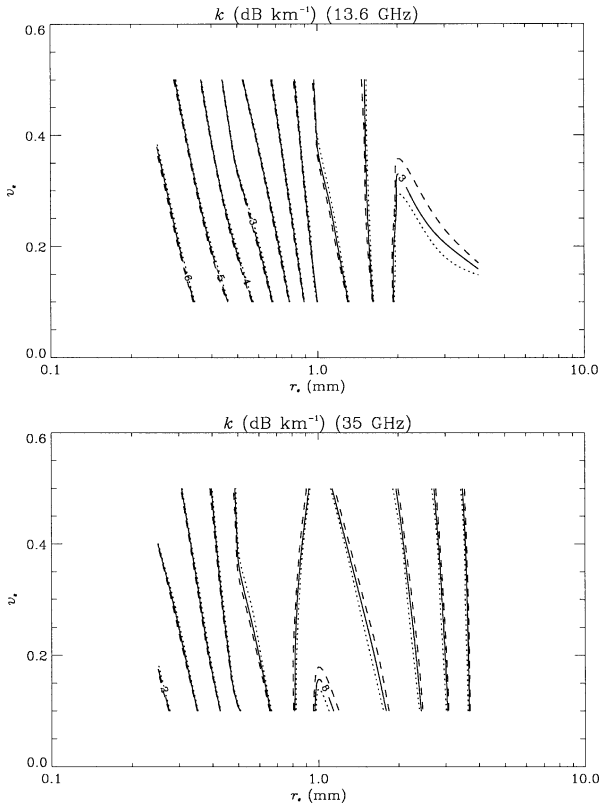

FIG. 7. Same as Fig. 3, except for specific attenuation.

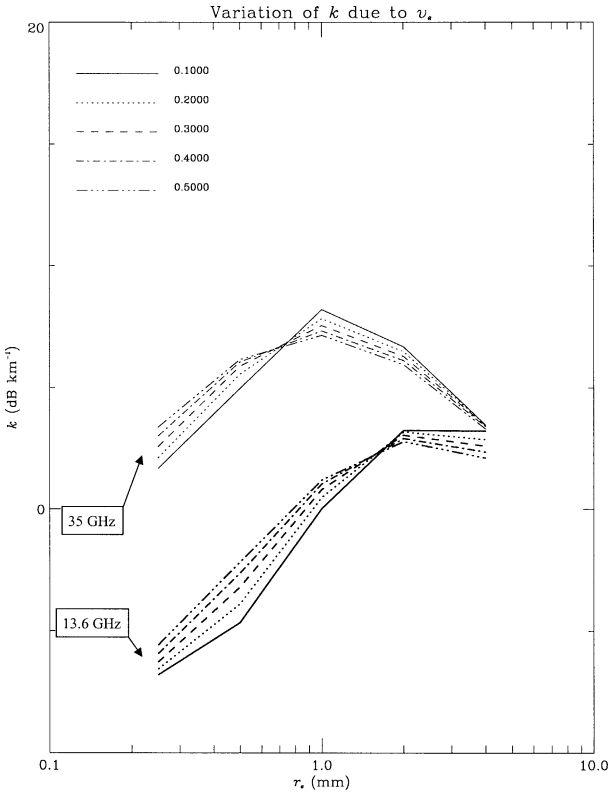

FIG. 8. Same as Fig. 4, except for specific attenuation.

among distributions in a more comprehensive manner. As before, the solid lines contour the average specific attenuations of the 15 distributions for each effective variance/radius pair, while the dotted and dashed lines contour the minimum and maximum values. Results for both 13.6 (upper panel) and 35 GHz (lower panel) are shown. The tightness among the lines of different line styles is even more pronounced than shown in Fig. 3, providing evidence that variations caused by differences in the DSDs are less in specific attenuations across the entire range of effective variance and radius under examination.

Figure 8 illustrates the variations of specific attenuations due to the variations of effective variance. The average specific attenuation over the 15 distributions for each effective variance/radius pair is the dependent variable. Different effective variances are represented by different line styles. Similar to the behavior of equivalent reflectivity factor, the curves flatten out as the effective variance increases. Also, the curves for 13.6 GHz are nearly monotonically increasing with effective radius, except for $r_e > 2$ mm, while the curves for 35 GHz are convex with maxima near $r_e \approx 1$ mm. Therefore, different effective radii may result in the same specific attenuation at the higher 35-GHz frequency.

Figures 9a–c examine the feasibility of dual-frequency retrieval using specific attenuations, similar to Figs. 5a–c in terms of equivalent reflective factors. The convention used for these diagrams are consistent with those used in Figs. 5a–c. We note that the resolvability between effective radii of 0.25 and 0.5 mm is limited even for $v_e = 0.5$, and becomes less so as effective variance decreases. The ''fold over'' phenomenon observed in reflectivity factors at $v_e = 0.1$ is already apparent for specific attenuations at $v_e = 0.3$. Therefore, given specific attenuations at these two frequencies leads to some difficulty in determining W and effective radius for a DSD with effective radius smaller than ~1 mm.

d. Estimated average Doppler velocity in calm air

Figure 10 follows the same convention used in Figs. 3 and 7, but shows the mean Doppler velocity in calm air, $\overline{v}_0$ as a function of r_e and v_e. As noted in section 2, the vertical velocity formulation of Atlas and Ulbrich (1977) is used to produce these results. Contour lines are 1 m s^{-1} apart. The most salient feature is that $\overline{v}_0$ can be accurately determined given r_e and v_e, although the accuracy for smaller values of r_e is less than that for larger values. Furthermore, if effective radius is held constant the variation in effective variance also exerts a greater impact, as much as 3 m s^{-1}, to the estimated $\overline{v_0}$ for smaller effective radii.

5. Discussion

It may seem, up to this point, that the choice of using effective radius and effective variance to represent the rain DSD is arbitrary. We present here a rationale for such a choice. If one defines the backscatter efficiency, $Q_b(\lambda, r)$, and approximates its radius dependence with a polynomial in r, that is,

$$\sigma_b(\lambda, r) = \pi r^2 Q_b(\lambda, r) \approx \pi r^2 \sum_{l=0}^{L} b_l(\lambda) r^l, \quad (20)$$

then the equivalent radar reflectivity factor can be approximated by

$$Z_e(\lambda) \approx \frac{10^6 \lambda^4}{\pi^5 |K_w|^2} \pi \sum_{l=0}^{L} b_l(\lambda) \int_{r_{\min}}^{r_{\max}} r^{2+l} n(r)\, dr. \quad (21)$$

There is little doubt that as the number of terms, $L + 1$, increases, the approximation becomes more accurate. Note that the expansion coefficients b_1 are dependent of wavelength; for simplicity, this dependence will be taken as understood in later discussion.

If we start with three terms—that is, $L = 2$—the approximation to Z_e becomes

$$Z_e \approx \frac{10^6 \lambda^4}{\pi^5 |K_w|^2} \pi \left[b_0 \int_{r_{\min}}^{r_{\max}} r^2 n(r)\, dr + b_1 \int_{r_{\min}}^{r_{\max}} r^3 n(r)\, dr + b_2 \int_{r_{\min}}^{r_{\max}} r^4 n(r)\, dr \right]. \quad (22)$$

Noting that each integral in the square brackets can be expressed in terms of W, r_e, and υ_e, that is,

$$\int r^2 n(r)\, dr = (3/4\pi\rho_w)(W/r_e), \quad (23a)$$

$$\int r^3 n(r)\, dr = (3/4\pi\rho_w) W, \quad (23b)$$

$$\int r^4 n(r)\, dr = (3/4\pi\rho_w) W r_e (\upsilon_e + 1), \quad (23c)$$

then by substitution and simplification, Eq. (22) becomes

$$Z_e \approx \frac{10^6 \lambda^4}{\pi^5 |K_w|^2} \frac{3}{4} \frac{1}{\rho_w} W \left[b_0 \frac{1}{r_e} + b_1 + b_2 r_e (\upsilon_e + 1) \right]. \quad (24)$$

Thus using W, r_e, and υ_e to estimate equivalent reflectivity factor is at the very least equivalent to approximating the backscatter efficiency using the first three terms of its polynomial expansion in r. Similarly, for the extinction cross section and extinction efficiency,

$$\sigma_e(\lambda, r) = \pi r^2 Q_e(\lambda, r) \approx \pi r^2 \sum_{l=0}^{L} e_l(\lambda) r^l, \quad (25)$$

and for the specific attenuation,

$$k \approx 0.434 \frac{3}{4} \frac{1}{\rho_w} W \left[e_0 \frac{1}{r_e} + e_1 + e_2 r_e (\upsilon_e + 1) \right]. \quad (26)$$

The above explanation is somewhat oversimplified, since regression analysis using Eqs. (20) and (25) for Q_b and Q_e and Eqs. (24) and (26) for Z_e and k does not lead to ideal parameter fits. Nonetheless, the analysis serves a heuristic purpose. The phenomenon that we observe—that is, Z_e and k can be accurately estimated given W, r_e, and υ_e—only requires that Z_e and k both be approximate functions of the latter, that is, $Z_e \approx Z_e(W, r_e, \upsilon_e)$ and $k \approx k(W, r_e, \upsilon_e)$. There is no requirement as to what form those functions assume. We find that a function involving the product of a linear function in W and an exponential function whose exponent is a third-degree polynomial in both r_e and υ_e works satisfactorily. The linear relationship of Z_e and k to W is natural. Since the total number concentration N_T is canceled out in calculations of r_e and υ_e, it only remains in W as it is in Z_e and k. Therefore, W, Z_e, and k all scale the same way by N_T.

It is now clear that Z_e and k are at least approximate functions of W, r_e, and υ_e. Ideally, we need three pieces of information in order to infer the three unknowns. However, with a dual-frequency radar system, there are only two pieces of information. Although it is a pragmatic choice, the shortcoming may be overcome by making reasonable assumptions concerning the interrelations among W, r_e, and υ_e. One may assume that the natual range of υ_e is small enough that it can be considered constant. However, this is not likely to be an effective assumption, especially when considering the rain-rate profile. For example, in considering the often subtle rain-rate variations with height, particularly in a time-dependent framework, it is hard to conceive that the DSDs would have the same breadth factor throughout the vertical column and rain development stages.

Thus another scenario for addressing the shortcoming is by assuming that the three parameters are not independent of each other. There is published evidence to this possibility (Haddad et al. 1996, 1997a), in which case one of the parameters may be expressed as the combination of the other two. The authors and their colleagues are currently examining existing DSD data for the validity of this behavior.

The results presented in the previous section suggest that, given good absolute calibration of a radar, reasonably accurate dual-frequency rain-rate retrieval can be expected. Since specific attenuation is a derived quantity that cannot be measured directly, the only direct measurements from the radar are the attenuated equivalent reflectivity factors or something equivalent. Therefore, dual-frequency retrieval methods either relate the equivalent reflectivity factors and specific attenuations to the rain rate (e.g., Fujita 1983) or relate them to specific models of size distribution (e.g., Meneghini et al. 1997). They then use a least squares method or a recursive

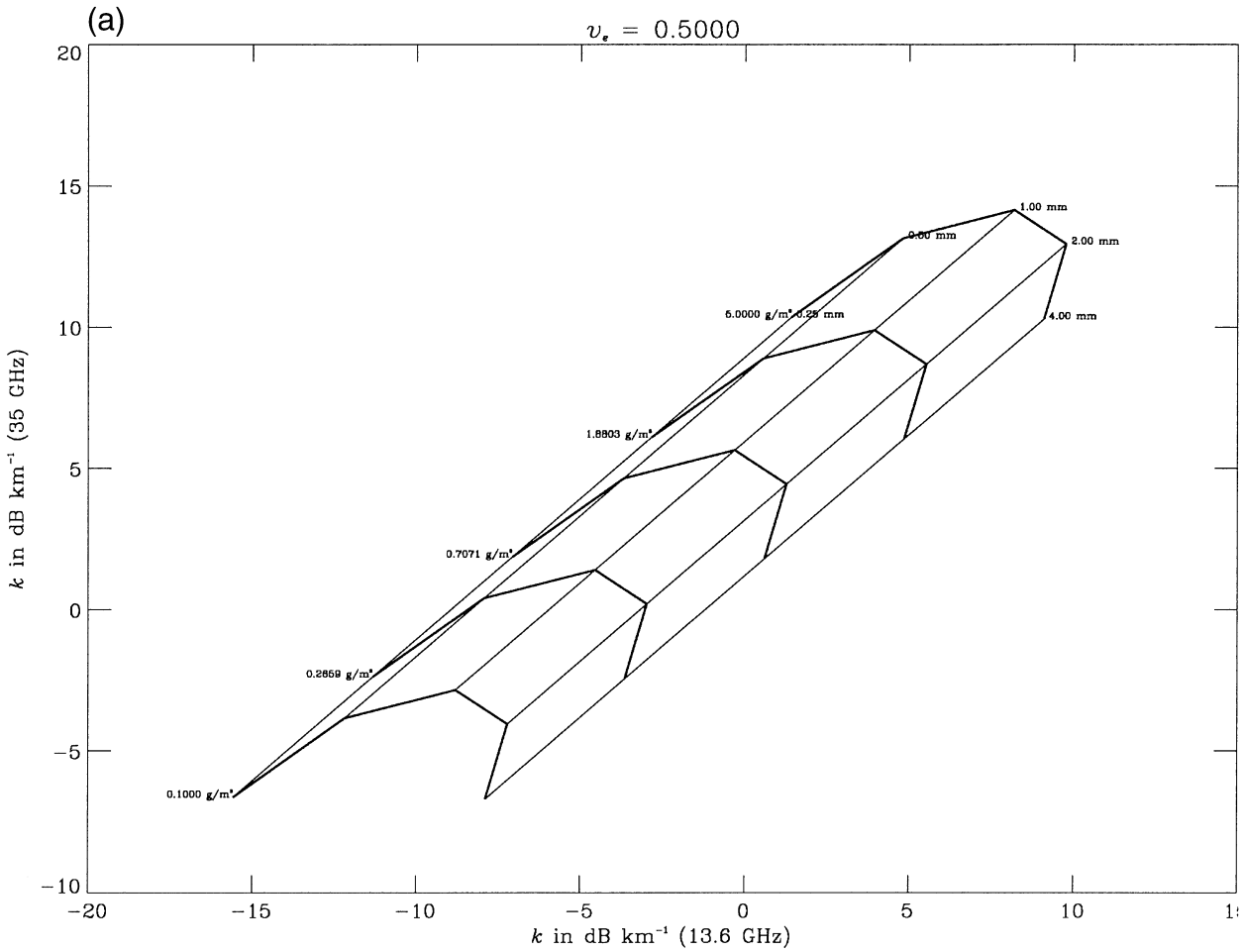

FIG. 9. Combined effects of liquid water content and effective radius on specific attenuations at both 13.6 (abscissa) and 35 GHz (ordinate) for effective variance of (a) 0.5, (b) 0.3, and (c) 0.1.

method to retrieve the desired rain rates or DSD parameters.

As indicated previously, the former approach ignores the fact that both equivalent reflectivity factor and specific attenuation do not contain raindrop fall velocity information necessary for evaluation of rain rate, that is, vertical rain mass flux. This lack of information is one of the major reasons for the myriad of reported *Z–R* and *k–R* relationships. By the same token, the latter approach is only applicable to the specific assumed DSD, and thus, once the real DSD deviates from the assumed there is no telling how the algorithm will perform.

Therefore, we propose to avoid assuming a specific distribution model and, instead, use liquid water content, effective radius, and effective variance as the parameters for specifying the DSD and other diagnostic parameters, since together they determine the equivalent reflectivity factor and specific attenuation in a manner insensitive to the details of the DSD. By the addition of estimated mean Doppler velocity for calm air, which can also be reasonably determined by these three parameters, we expect improvements in rain-rate estimates once the capability of estimating $\overline{v}$ becomes available from spaceborne precipitation radars.

The results also show that the accuracy of the retrievals based on this three-parameter approach would be expected to decrease as the effective radius of the distribution becomes smaller. This is also where ambiguities in both equivalent reflectivity factor and specific attenuation occur and where uncertainty in $\overline{v}_0$ is largest—corresponding to light rain situations. We submit that reported inaccuracies in light rain retrieval in current TRMM algorithms is a manifestation of the same effect; see Smith et al. (1998) for a discussion of the light rain problem in the radiometer algorithm framework and Meneghini et al. (2000) for a discussion of this same problem vis-à-vis the TRMM PR algorithm framework. This deficiency is inherent to the current rain observing instrument and is not, necessarily, caused by the choice of algorithm parameters.

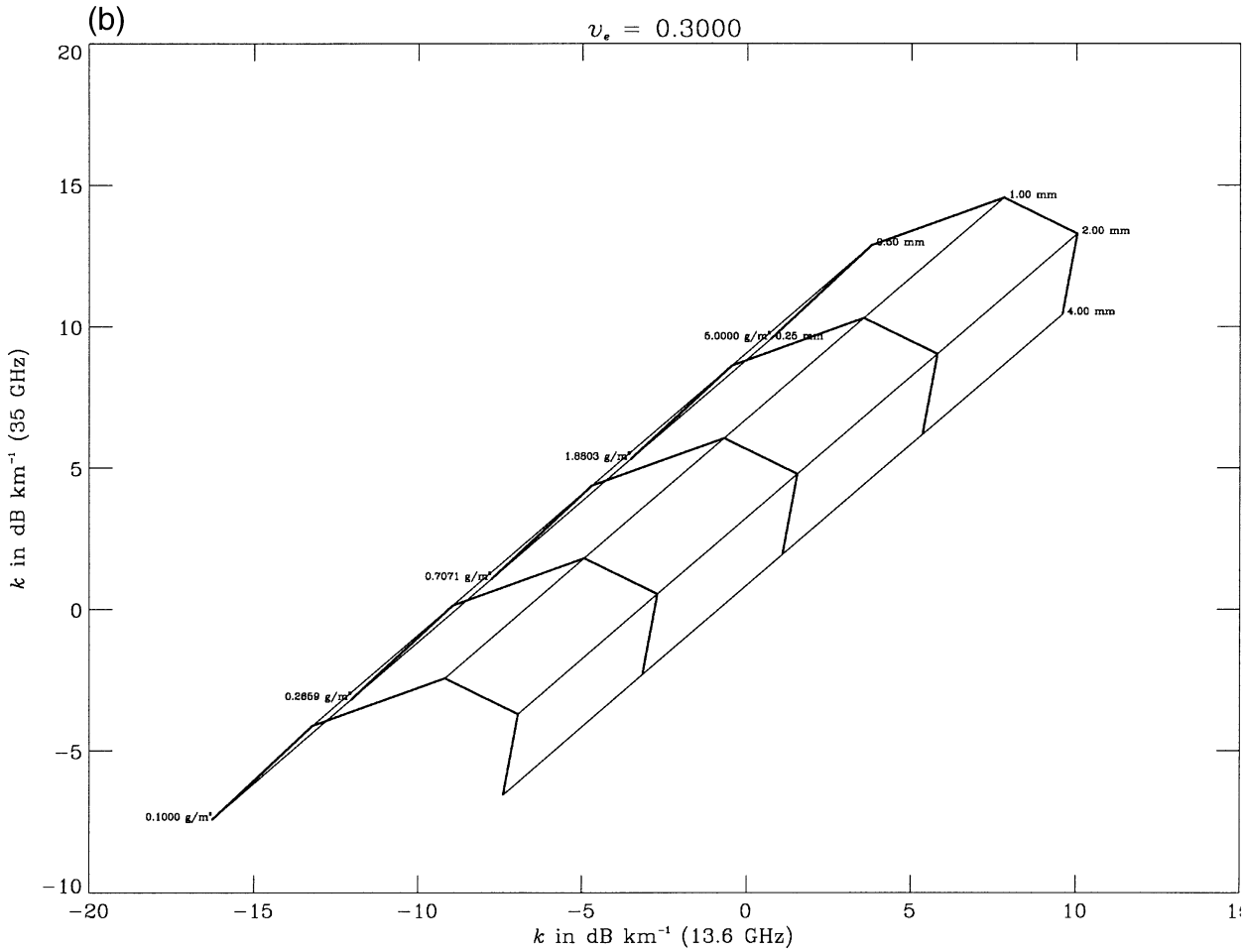

FIG. 9. (*Continued*)

6. Conclusions

In this study we establish a theoretically sound framework in which improved rain-rate retrieval may be achieved using a dual-frequency spaceborne radar, with the addition of a broadband Doppler capability. At the center of this framework is the use of liquid water content, effective radius, and effective variance as the parameter set that best specifies drop size distribution and the related rain-rate parameter. It is shown that both equivalent reflectivity factor and specific attenuation are accurately determined by this set of parameters in which the influence of the details of size distribution to the two radar parameters becomes inconsequential. They therefore provide a more robust basis for radar rainfall retrieval than methods based on ad hoc *Z–R* and *k–R* relationships or methods based on specific drop size distribution models.

Furthermore, this triad of parameters nicely predicts the mean Doppler velocity $\overline{v}_0$ in calm air. Using this parameter along with the first moment of the measured Doppler spectrum, one can further estimate the updraft and, in turn, incorporate the updraft into the estimation of in-cloud rain mass flux. This is an improvement over the current methods that do not take this factor into account.

Given that the next dedicated satellite precipitation mission, that is, the Global Precipitation Measurement mission, will incorporate a dual-frequency Ku–Ka-band radar for the main purpose of providing sensitivity to horizontal and vertical variations in the drop size distribution, it is important to optimize future algorithms used to quantify these variations. This analysis offers a step in that direction. The investigation has also looked beyond the initial GPM mission era to a time when Doppler capability will be added to spaceborne rain radars, commencing an era when strong precipitating updrafts and downdrafts can be differentiated and even greater understanding of dynamical and diabatic thermal processes within precipitating clouds can be achieved.

Acknowledgments. This research has been supported by the NASA Goddard Space Flight Center Global Precipitation Measurement (GPM) mission formulation project under the auspices of Codes 420.2 and 912. The

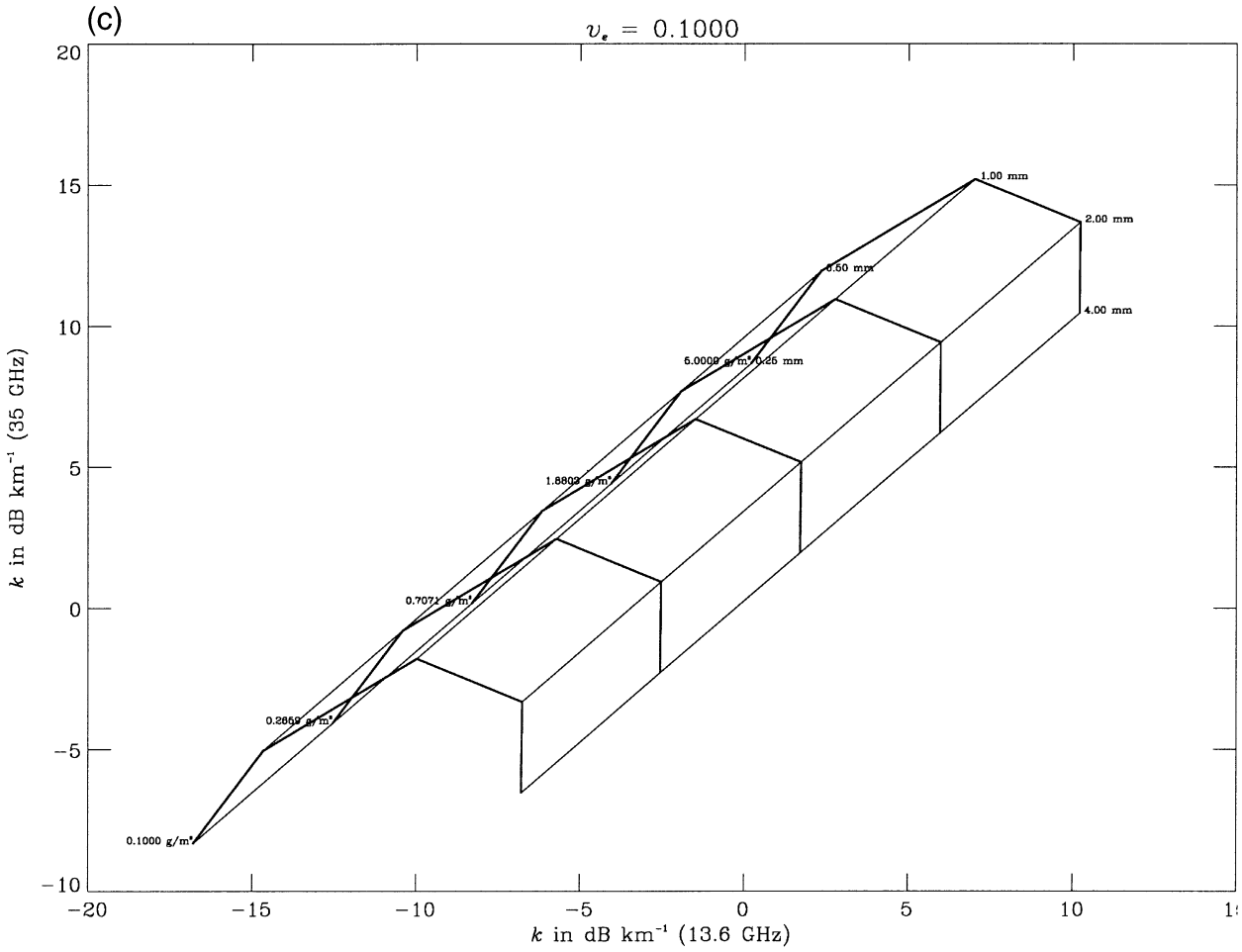

FIG. 9. (*Continued*)

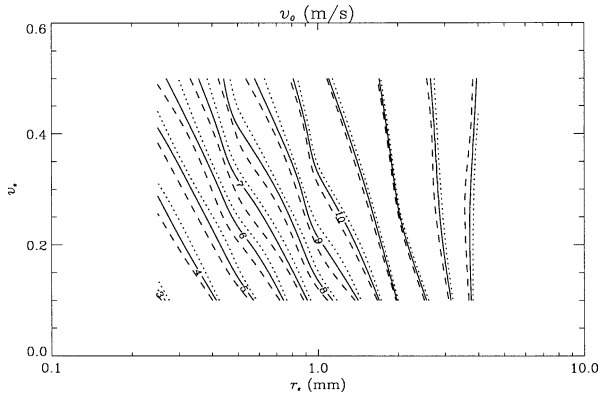

FIG. 10. Contours of mean Doppler velocity in calm air as a function of effective radius and effective variance while holding liquid water content constant at 1 g m^{-3}. Solid contours are the mean of 15 distributions, while dotted and dashed contours denote the minimum and maximum, respectively.

authors express their appreciation to a number of members from the TRMM Science Team for helpful discussions and debate.

APPENDIX A

Bimodal Modified Gamma Distribution

The modified gamma distribution defined in Deirmendjian (1969) has the following form:

$$n(r) = ar^{\mu} \exp(-br^{\kappa}), \tag{A1}$$

where a, b, μ, and $\kappa > 0$. Defining the characteristic radius as

$$r_c = \left(\frac{1}{b}\right)^{1/\kappa} \tag{A2}$$

leads to

$$n(r) = ar^{\mu} \exp\left[-\left(\frac{r}{r_c}\right)^{\kappa}\right]. \tag{A3}$$

Recalling the definition of the incomplete gamma function,

$$\gamma(x,\,\alpha) \equiv \int_0^{\alpha} t^{x-1}e^{-t}\,dt, \tag{A4}$$

the total number concentration N_T of the distribution is found to be

$$N_T = \int_{r_{\min}}^{r_{\max}} n(r)\,dr = a\kappa^{-1}r_c^{\mu+1}\left[\gamma\left(\frac{\mu+1}{\kappa},\, z_{\max}\right) - \gamma\left(\frac{\mu+1}{\kappa},\, z_{\min}\right)\right], \tag{A5}$$

where $r_{\max}$ ($r_{\min}$) are the maximum (minimum) radius considered in the distribution, $z_{\max} = (r_{\max}/r_c)^{\kappa}$, and similarly $z_{\min} = (r_{\min}/r_c)^{\kappa}$. Letting

$$G\left(\frac{\mu+1}{\kappa},\, z_{\min},\, z_{\max}\right) \equiv \left[\gamma\left(\frac{\mu+1}{\kappa},\, z_{\max}\right) - \gamma\left(\frac{\mu+1}{\kappa},\, z_{\min}\right)\right], \tag{A6}$$

then constant a becomes

$$a = G\left(\frac{\mu+1}{\kappa},\, z_{\min},\, z_{\max}\right)^{-1}\kappa N_T r_c^{-(\mu+1)}. \tag{A7}$$

This results in the form of the modified gamma distribution used in the bimodal modified gamma distribution

$$n(r) = G\left(\frac{\mu+1}{\kappa},\, z_{\min},\, z_{\max}\right)^{-1} \times \kappa\left(\frac{r}{r_c}\right)^{\mu}\exp\left[-\left(\frac{r}{r_c}\right)^{\kappa}\right]\left(\frac{N_T}{r_c}\right). \tag{A8}$$

Note that, except for the last term in the parentheses, all other terms are dimensionless. The units of $n(r)$ therefore only depend on the units of N_T and r_c, which makes the expression convenient. Moreover,

$$\lim_{\alpha\to\infty}\gamma(x,\,\alpha) = \Gamma(x) = \int_0^{\infty} t^{x-1}e^{t}\,dt. \tag{A9}$$

That is, if the range of raindrop size is unlimited, the incomplete gamma function is replaced with the regular gamma function. If κ is set to one, the modified gamma distribution is reduced to the regular gamma distribution. If, in addition, μ is set to zero, the distribution is further reduced to the exponential distribution.

The integral of the modified gamma distribution multiplied by some power of r results in

$$\int_{r_{\min}}^{r_{\max}} r^{p}n(r)\,dr = \frac{G\left(\frac{\mu+p+1}{\kappa},\, z_{\min},\, z_{\max}\right)}{G\left(\frac{\mu+1}{\kappa},\, z_{\min},\, z_{\max}\right)}N_T r_c^{p}, \tag{A10}$$

from which one may quickly find the moments of the distribution.

The bimodal modified gamma distribution used in this study is a combination of two modified gamma distributions with the same μ and κ, but different characteristic radii:

$$n(r) = G\left(\frac{\mu+1}{\kappa},\, z_{1,\min},\, z_{1,\max}\right)^{-1} \times \kappa\left(\frac{r}{r_{c,1}}\right)^{\mu}\exp\left[-\left(\frac{r}{r_{c,1}}\right)^{\kappa}\right]\left(\frac{fN_T}{r_{c,1}}\right) + G\left(\frac{\mu+1}{\kappa},\, z_{2,\min},\, z_{2,\max}\right)^{-1} \times \kappa\left(\frac{r}{r_{c,2}}\right)^{\mu}\exp\left[-\left(\frac{r}{r_{c,2}}\right)^{\kappa}\right]\left[\frac{(1-f)N_T}{r_{c,2}}\right], \tag{A11}$$

where $r_{c,1} < r_{c,2}$ and the fraction f of the total number concentration is in the modified gamma distribution with characteristic radius $r_{c,1}$. It is clear that this definition of bimodal modified gamma distribution incorporates the single modified gamma distribution. To achieve this, one only needs to set $f = 1$ and $r_{c,1} = r_c$.

The integral of the bimodal modified gamma distribution multiplied by the radius raised to some power p becomes

$$\int_{r_{\min}}^{r_{\max}} r^{p}n(r)\,dr = f\frac{G\left(\frac{\mu+p+1}{\kappa},\, z_{1,\min},\, z_{1,\max}\right)}{G\left(\frac{\mu+1}{\kappa},\, z_{1,\min},\, z_{1,\max}\right)}N_T r_{c,1}^{p} + (1-f)\frac{G\left(\frac{\mu+p+1}{\kappa},\, z_{2,\min},\, z_{2,\max}\right)}{G\left(\frac{\mu+1}{\kappa},\, z_{2,\min},\, z_{2,\max}\right)}N_T r_{c,2}^{p}$$

$$= \left[f \frac{G\left(\frac{\mu + p + 1}{\kappa}, z_{1,\min}, z_{1,\max}\right)}{G\left(\frac{\mu + 1}{\kappa}, z_{1,\min}, z_{1,\max}\right)} + (1 - f) \frac{G\left(\frac{\mu + p + 1}{\kappa}, z_{2,\min}, z_{2,\max}\right)}{G\left(\frac{\mu + 1}{\kappa}, z_{2,\min}, z_{2,\max}\right)} \left(\frac{r_{c,2}}{r_{c,1}}\right)^p \right] N_T r_{c,1}^p, \quad \text{(A12)}$$

where $z_{1,\max} = (r_{\max}/r_{c,1})^\kappa$ and similarly for $z_{1,\min}$, $z_{2,\max}$, and $z_{2,\min}$. Also, define

$$H(p) \equiv f \frac{G\left(\frac{\mu + p + 1}{\kappa}, z_{1,\min}, z_{1,\max}\right)}{G\left(\frac{\mu + 1}{\kappa}, z_{1,\min}, z_{1,\max}\right)} + (1 - f) \frac{G\left(\frac{\mu + p + 1}{\kappa}, z_{2,\min}, z_{2,\max}\right)}{G\left(\frac{\mu + 1}{\kappa}, z_{2,\min}, z_{2,\max}\right)} \left(\frac{r_{c,2}}{r_{c,1}}\right)^p, \quad \text{(A13)}$$

where the dependence of H on the other variables is implied. In actuality,

$$H(p) \equiv H\left(p, f, \mu, \kappa, r_{c,1}, \frac{r_{c,2}}{r_{c,1}}, r_{\min}, r_{\max}\right). \quad \text{(A14)}$$

Therefore,

$$\int_{r_{\min}}^{r_{\max}} r^p n(r)\, dr = H(p) N_T r_{c,1}^p. \quad \text{(A15)}$$

Using this formula, the liquid water content becomes

$$W = \frac{4}{3}\pi\rho_w \int_{r_{\min}}^{r_{\max}} r^3 n(r)\, dr = \frac{4}{3}\pi\rho_w H(3) N_T r_{c,1}^3, \quad \text{(A16)}$$

where ρ_w is the density of water. The effective radius and variance are, respectively,

$$r_e = \frac{\int_{r_{\min}}^{r_{\max}} r^3 n(r)\, dr}{\int_{r_{\min}}^{r_{\max}} r^2 n(r)\, dr} = \frac{H(3)}{H(2)} r_{c,1} \quad \text{and} \quad \text{(A17a)}$$

$$v_e = \frac{\int_{r_{\min}}^{r_{\max}} r^4 n(r)\, dr}{r_e^2 \int_{r_{\min}}^{r_{\max}} r^2 n(r)\, dr} - 1 = \frac{H(4)}{H(2)} r_{c,1}^2 \left[\frac{H(2)}{H(3) r_{c,1}}\right]^2 - 1$$

$$= \frac{H(2)H(4)}{[H(3)]^2} - 1. \quad \text{(A17b)}$$

APPENDIX B

Estimation of Mean Doppler Velocity in Stagnant Air

The derivation below partly follows that of Rogers (1984). Readers may also refer to Meneghini and Kozu (1990, 63–70). The mean power received at the radar from range r, denoted by $\overline{P}_r$, can be expressed as the integral of the power distribution over the Doppler frequencies:

$$\overline{P}_r = \int_{-\infty}^{\infty} P_r(f)\, df, \quad \text{(B1)}$$

where $P_r(f)$ is the distribution of the short-term average signal power with respect to Doppler frequency. In practice, $\overline{P}_r$ is measured by ordinary incoherent means independently of the Doppler spectrum. The measured Doppler spectrum, $p_r(f)$ is proportional to $P_r(f)$ with the proportionality determined by $\overline{P}_r$. For convenience, the normalization of $p_r(f)$ is set to

$$\int_{-\infty}^{\infty} p_r(f)\, df = 1 \quad \text{(B2)}$$

so that

$$P_r(f) = \overline{P}_r p_r(f). \quad \text{(B3)}$$

The Doppler frequency is related to the velocity vector $\mathbf{V}$ of the moving scatterer by

$$f = -2\mathbf{V} \gg \hat{r}/\lambda, \quad \text{(B4)}$$

where λ is the radar wavelength, and $\hat{r}$is the unit vector directed outward from the radar to the target. The radial velocity component $v = -\mathbf{V} \cdot \hat{\mathbf{r}}$ is called the Doppler velocity. As defined here, a positive Doppler velocity corresponds to motion toward the radar. The scatterers illuminated by a radar pulse generally move with different speeds as a result of wind shear, turbulence, and differential fall velocities relative to the air, inducing a spectrum of Doppler frequencies instead of a single frequency.

Because of the one-to-one relationship between Doppler frequency and Doppler velocity, it is convenient to interpret the Doppler spectrum in terms of velocity. We therefore denote the spectrum as $W(v)$, which is related to $P_r(f)$ by

$$W(v) = P_r(f) \left|\frac{df}{dv}\right|. \quad \text{(B5)}$$

The function $W(v)$ indicates the distribution of received power as a function of radial velocity. In terms of properties of the scatterers, $W(v)$ also may be written as

$$W(v) = \zeta \int_0^\infty \sigma_b \phi(\sigma_b, v)\, d\sigma_b, \tag{B6}$$

where $\phi(\sigma_b, v)d\sigma_b dv$ is the joint probability that a randomly selected scatterer has a radial velocity between v and $v + dv$ and a radar backscatter cross section between σ_b and $\sigma_b + d\sigma_b$. The normalization factor ζ ensures that the integral of $W(v)$ equals the mean signal power.

For a vertically viewing radar, the Doppler velocities arise from the combined effects of vertical air motion and particle fall velocity. In this case, the joint probability $\phi(\sigma_b, v)$ may be expressed as the product of the probability distribution of radar backscatter cross section and the conditional probability of a velocity given by σ_b. That is,

$$\phi(\sigma_b, v) = \phi(\sigma_b)\phi(v/\sigma_b) = \phi(\sigma_b)\phi_{\sigma_b}(v), \tag{B7}$$

where $\phi_{\sigma_b} = \phi(v|\sigma_b)$ denotes conditional probability upon a given σ_b.

For particles such as dry snowflakes that have terminal fall speeds close to 1 m s^{-1} regardless of size, it is a reasonable approximation to suppose that the vertical velocities of the precipitation particles are uncorrelated with their size. The conditioning upon σ_b of ϕ_{σ_b} may then be neglected, in which $\phi(\sigma_b, v)$ can be factored into the separate probabilities of σ_b and v, leading to

$$W(v) = \zeta \phi(v)\overline{\sigma}_b, \tag{B8}$$

where $\overline{\sigma}_b = \int_0^\infty \sigma_b \phi(\sigma_b)\, d\sigma_b$ is the mean backscatter cross section of the snowflakes in the resolution volume. Thus, the Doppler spectrum is simply proportional to the velocity distribution of the particles. Since the integral of $W(v)$ over velocity equals the mean power $\overline{P}_r$, it follows that the normalization factor must be

$$\zeta = \frac{\overline{P}_r}{\overline{\sigma}_b}. \tag{B9}$$

As another special case, suppose that there is a one-to-one relationship between the vertical velocity of a scatterer and its radar cross section. This is a reasonable approximation for falling raindrops, small in comparison to the wavelength, because terminal fall speed and radar backscatter cross section are both increasing functions of drop size. The conditional probability distribution may then be written as

$$\phi_{\sigma_b}(v) = \delta[v - v_0(\sigma_b)], \tag{B10}$$

where δ is the Dirac delta function, and v_0 is the velocity corresponding to backscatter cross section σ_b in still air. Accordingly, the Doppler spectrum is given by

$$W(v) = \frac{\overline{P}_r}{\overline{\sigma}_b} \int_0^\infty \sigma_b \phi(\sigma_b)\delta[v - v_0(\sigma_b)]\, d\sigma_b. \tag{B11}$$

For raindrops it is helpful to introduce drop diameter as an independent variable instead of σ_b. The $\phi(\sigma_b)$ may be replaced by the drop size distribution function $N(D)$ by using the relationship

$$\phi(\sigma_b)d\sigma_b = \frac{1}{N_T} N(D)dD. \tag{B12}$$

Given this relationship,

$$W(v) = \frac{\overline{P}_r}{\eta} \int_0^\infty \sigma_b(D)N(D)\delta[v - v_0(D)]\, dD, \tag{B13}$$

where $\eta = N_T\overline{\sigma}_b$ is the reflectivity per unit volume of rain. The integration can be carried out by substituting $dD = (dD/dv_0)dv_0$, whence

$$W(v) = \frac{\overline{P}_r}{\eta}\left\{\sigma_b[D(v_0)]N[D(v_0)]\frac{dD}{dv_0}\right\}_{v_0=v}. \tag{B14}$$

This formula is used in this study to estimate the mean Doppler velocity in calm air.

REFERENCES

Amayenc, P., J. Testud, and M. Marzoug, 1993: Proposal for a spaceborne dual-beam rain radar with Doppler capability. *J. Atmos. Oceanic Technol.*, **10,** 262–276.

Atlas, D., 1954: The estimation of cloud parameters by radar. *J. Meteor.*, **11,** 309–317.

——, and A. C. Chmela, 1957: Physical-synoptic variations of drop-size parameters. Preprints, *Sixth Weather Radar Conference*, Boston, MA, Amer. Meteor. Soc., 21–30.

——, and C. W. Ulbrich, 1977: Path- and area-integrated rainfall measurement by microwave attenuation in the 1–3 cm band. *J. Appl. Meteor.*, **16,** 1322–1331.

——, ——, and R. Meneghini, 1984: The multiparameter remote measurement of rainfall. *Radio Sci.*, **19,** 3–22.

Battan, L. J., 1973: *Radar Observation of the Atmosphere*. University of Chicago Press, 324 pp.

Chandrasekar, V., E. Gorgucci, and G. Scarchilli, 1993: Optimization of multiparameter radar estimates of rainfall. *J. Appl. Meteor.*, **32,** 1288–1293.

Czerwinski, N., and W. Pfisterer, 1972: Types of raindrop spectra of polar to tropic zones and their dependence on rain elements. *Meteor. Rundsch.*, **25,** 88–94.

Deirmendjian, D., 1969: *Electromagnetic Scattering on Spherical Polydispersions*. Elsevier, 291 pp.

Durden, S. L., E. Im, F. K. Li, W. Ricketts, A. Tanner, and W. Wilson, 1994: ARMAR: An airborne rain mapping radar. *J. Atmos. Oceanic Technol.*, **11,** 727–737.

Eccles, P. J., 1979: Comparison of remote measurements by single- and dual-wavelength meteorological radars. *IEEE Trans. Geosci. Remote Sens.*, **17,** 205–218.

——, and E. A. Mueller, 1971: X-band attenuation and liquid water content estimation by a dual-wavelength radar. *J. Appl. Meteor.*, **10,** 1252–1259.

Fujita, M., 1983: An algorithm for estimating rain rate by a dual-frequency radar. *Radio Sci.*, **18,** 697–708.

——, K. Okamoto, S. Yoshikado, and K. Nakamura, 1985: Inference of rain rate profile and path-integrated rain rate by an airborne microwave scatterometer. *Radio Sci.*, **20,** 631–642.

Goldhirsh, J., and I. Katz, 1974: Estimation of raindrop size distri-

bution using multiple wavelength radar systems. *Radio Sci.,* **9,** 439–446.

Gossard, E. E., R. G. Strauch, D. C. Welsh, and S. Y. Matrosov, 1992: Cloud layers, particle identification, and rain-rate profiles from ZRVf Measurements by clear-air Doppler radars. *J. Atmos. Oceanic Technol.,* **9,** 108–119.

Gunn, R., and G. D. Kinzer, 1949: The terminal velocity of fall for water droplets in stagnant air. *J. Meteor.,* **6,** 243–248.

Haddad, Z. S., E. Im, and S. L. Durden, 1995: Intrinsic ambiguities in the retrieval of rain rates from radar returns at attenuating wavelengths. *J. Appl. Meteor.,* **34,** 2667–2679.

——, S. L. Durden, and E. Im, 1996: Parameterizing the raindrop size distribution. *J. Appl. Meteor.,* **35,** 3–13.

——, D. A. Short, S. L. Durden, E. Im, S. Hensley, M. B. Grable, and R. A. Black, 1997a: A new parameterization of the rain drop size distribution. *IEEE Trans. Geosci. Remote Sens.,* **35,** 532–539.

——, E. A. Smith, C. D. Kummerow, T. Iguchi, M. R. Farrar, S. L. Durden, M. Alves, and W. S. Olson, 1997b: The TRMM ''Day-1'' radar/radiometer combined rain-profiling algorithm. *J. Meteor. Soc. Japan,* **75,** 799–809.

Hansen, J. E., and L. D. Travis, 1974: Light scattering in planetary atmosphere. *Space Sci. Rev.,* **16,** 527–610.

Iguchi, T., and R. Meneghini, 1994: Intercomparison of single-frequency methods for retrieving a vertical rain profile from airborne or spaceborne radar data. *J. Atmos. Oceanic Technol.,* **11,** 1507–1516.

——, T. Kozu, R. Meneghini, J. Awaka, and K. Okamoto, 2000: Rain-profiling algorithm for the TRMM precipitation radar. *J. Appl. Meteor.,* **39,** 2038–2052.

Im, E., and Coauthors, 2002: Second-Generation Precipitation Radar (PR-2). Final Rep. JPL D-22997, NASA Earth Science Instrument Incubator Program, Jet Propulsion Laboratory, California Institute of Technology, Pasadena, CA, 164 pp.

Kozu, T., and K. Nakamura, 1991: Rainfall parameter estimation from dual-radar measurements combining reflectivity profile and path-integrated attenuation. *J. Atmos. Oceanic Technol.,* **8,** 259–270.

——, ——, R. Meneghini, and W. C. Boncyk, 1991: Dual-parameter radar rainfall measurement from space: A test result from an aircraft experiment. *IEEE Trans. Geosci. Remote Sens.,* **29,** 690–703.

——, and Coauthors, 2001: Development of precipitation radar onboard the Tropical Rainfall Measuring Mission (TRMM) satellite. *IEEE Trans. Geosci. Remote Sens.,* **GE-39,** 102–143.

Kummerow, C., W. Barnes, T. Kozu, J. Shiue, and J. Simpson, 1998: The Tropical Rainfall Measuring Mission (TRMM) sensor package. *J. Atmos. Oceanic Technol.,* **15,** 809–817.

Lhermitte, R. M., 1988: Cloud and precipitation remote sensing at 94 GHz. *IEEE Trans. Geosci. Remote Sens.,* **26,** 207–216.

Li, L., E. Im, S. L. Durden, and Z. S. Haddad, 2002: A surface wind model-based method to estimate rain-induced radar path attenuation over ocean. *J. Atmos. Oceanic Technol.,* **19,** 658–672.

Marshall, J. S., and W. M. K. Palmer, 1948: The distribution of raindrops with size. *J. Meteor.,* **5,** 165–166.

Marzoug, M., and P. Amayenc, 1991: Improved range-profiling algorithm of rainfall rate from a spaceborne radar with path-integrated attenuation constraint. *IEEE Trans. Geosci. Remote Sens.,* **29,** 584–592.

——, and ——, 1994: A class of single- and dual-frequency algorithms for rain-rate profiling from a spaceborne radar. Part I: Principle and tests from numerical simulations. *J. Atmos. Oceanic Technol.,* **11,** 1480–1506.

Meneghini, R., and T. Kozu, 1990: *Spaceborne Weather Radar.* Artech House, 199 pp.

——, J. Eckerman, and D. Atlas, 1983: Determination of rain rate from a spaceborne radar using measurements of total attenuation. *IEEE Trans. Geosci. Remote Sens.,* **21,** 34–43.

——, J. A. Jones, and L. H. Gesell, 1987: Analysis of a dual-wavelength surface reference radar technique. *IEEE Trans. Geosci. Remote Sens.,* **25,** 456–471.

——, T. Kozu, H. Kumagai, and W. C. Boncyk, 1992: A study of rain estimation methods from space using dual-wavelength radar measurements at near-nadir incidence over ocean. *J. Atmos. Oceanic Technol.,* **9,** 364–382.

——, H. Kumagai, J. R. Wang, T. Iguchi, and T. Kozu, 1997: Microphysical retrievals over stratiform rain using measurements from an airborne dual-wavelength radar-radiometer. *IEEE Trans. Geosci. Remote Sens.,* **35,** 487–506.

——, T. Iguchi, T. Kozu, L. Liao, K. Okamoto, J. Jones, and J. Kwiatkowski, 2000: Use of the surface reference technique for path attenuation estimates from the TRMM Precipitation Radar. *J. Appl. Meteor.,* **39,** 2053–2070.

——, L. Liao, S. W. Bidwell, and G. M. Heymsfield, 2001: On the feasibility of Doppler weather radar for estimates of drop size distribution using two closely-spaced frequencies. *IEEE Trans. Geosci. Remote Sens.,* **39,** 2203–2216.

Nakamura, K., and H. Inomata, 1992: Dual-polarization rain observation by X-band and Ka-band dual wavelength radar. *J. Meteor. Soc. Japan,* **70,** 762–768.

——, K. Okamoto, and T. Ihara, 1990: Conceptual design of rain radar for the Tropical Rainfall Measuring Mission. *Int. J. Satellite Commun.,* **8,** 257–268.

Okamoto, K., J. Awaka, and T. Kozu, 1988: A feasibility study of rain radar for the Tropical Rainfall Measuring Mission. 6: A case study of rain radar system. *J. Commun. Res. Lab.,* **35,** 183–208.

——, and Coauthors, 2001: *Global Environment Remote Sensing* (translated from Japanese). Ohmsha Press, 308 pp.

Petersen, W. A., and S. A. Rutledge, 2001: Regional variability in tropical convection: Observations from TRMM. *J. Climate,* **14,** 3566–3586.

Rogers, R. R., 1984: A review of multiparameter radar observations of precipitation. *Radio Sci.,* **19,** 23–36.

Shin, D.-B., G. R. North, and K. Bowman, 2000: A summary of reflectivity profiles from the first year of TRMM radar data. *J. Climate,* **13,** 4072–4086.

Short, D. A., and K. Nakamura, 2000: TRMM radar observations of shallow precipitation over the tropical oceans. *J. Climate,* **13,** 4107–4124.

Smith, E. A., J. Turk, M. Farrar, A. Mugnai, and X. Xiang, 1997: Estimating 13.8-GHz path-integrated attenuation from 10.7-GHz brightness temperatures for the TRMM combined PR–TMI precipitation algorithm. *J. Appl. Meteor.,* **36,** 365–388.

——, and Coauthors, 1998: Results of WetNet PIP-2 project. *J. Atmos. Sci.,* **55,** 1483–1536.

——, and Coauthors, 2004: International Global Precipitation Measurement (GPM) Program and Mission: An overview. *Measuring Precipitation from Space: EURAINSAT and the Future,* V. Levizzani and F. J. Turk, Eds., Kluwer, in press.

Spilhaus, A. F., 1948: Drop size intensity and radar echo of rain. *J. Meteor.,* **5,** 161–164.

Tanelli, S., E. Im, S. L. Durden, L. Facheris, and D. Giuli, 2002: The effects of nonuniform beam filling on vertical rainfall velocity measurements with a spaceborne Doppler radar. *J. Atmos. Oceanic Technol.,* **19,** 1019–1034.

Testud, J., P. Amayenc, and M. Marzoug, 1992: Rainfall-rate retrieval from a spaceborne radar: Comparison between single frequency, dual-frequency, and dual-beam techniques. *J. Atmos. Oceanic Technol.,* **9,** 599–623.

——, S. Oury, R. A. Black, P. Amayenc, and X. Dou, 2001: The concept of ''normalized'' distribution to describe raindrop spectra: A tool for cloud physics and remote sensing. *J. Appl. Meteor.,* **40,** 1118–1140.

Twomey, S., 1953: On the measurement of precipitation intensity by radar. *J. Meteor.,* **10,** 66–67.

Ulbrich, C. W., 1983: Natural variations in the analytical form of the raindrop size distribution. *J. Climate Appl. Meteor.,* **22,** 1764–1775.

——, 1986: A review of the differential reflectivity technique of measuring rainfall. *IEEE Trans. Geosci. Remote Sens.*, **GE-24,** 955–965.

——, 1992: Effects of drop-size-distribution truncation on computer simulations of dual-measurement radar methods. *J. Appl. Meteor.*, **31,** 689–699.

——, and D. Atlas, 1977: A method for measuring precipitation parameters using radar reflectivity and optical extinction. *Ann. Telecommun.*, **32,** 415–421.

Walker, G. B., L. S. Lamberth, and J. J. Stephens, 1964: Dual-frequency radar observations of precipitation. *J. Appl. Meteor.*, **3,** 430–438.